KUOPION YLIOPISTON JULKAISUJA C. LUONNONTIETEET JA YMPÄRISTÖTIETEET 205
KUOPIO UNIVERSITY PUBLICATIONS C. NATURAL AND ENVIRONMENTAL SCIENCES 205

SIMO SAARAKKALA

Pre-Clinical Ultrasound Diagnostics of Articular Cartilage and Subchondral Bone

Doctoral dissertation

To be presented by permission of the Faculty of Natural and Environmental Sciences
of the University of Kuopio for public examination in Auditorium L21,
Snellmania building, University of Kuopio,
on Friday 2nd February 2007, at 12 noon

Department of Physics, University of Kuopio
Department of Anatomy, University of Kuopio
Department of Clinical Physiology and Nuclear Medicine,
Kuopio University Hospital and University of Kuopio

KUOPION YLIOPISTO
KUOPIO 2007

Distributor:
Kuopio University Library
P.O. Box 1627
FI-70211 KUOPIO
FINLAND
Tel. +358 17 163 430
Fax +358 17 163 410
http://www.uku.fi/kirjasto/julkaisutoiminta/julkmyyn.html

Series Editors:
Professor Pertti Pasanen, Ph.D.
Department of Environmental Sciences

Professor Jari Kaipio, Ph.D.
Department of Physics

Author's address:
Department of Clinical Radiology
Kuopio University Hospital
P.O. Box 1777
FI-70211 KUOPIO
FINLAND
Tel. +358 44 717 4390
Fax +358 17 173 341
E-mail: simo.saarakkala@uku.fi

Supervisors:
Professor Jukka Jurvelin, Ph.D.
Department of Physics
University of Kuopio

Docent Juha Töyräs, Ph.D.
Department of Clinical Neurophysiology
Kuopio University Hospital

Professor Heikki Helminen, M.D., Ph.D.
Department of Anatomy
University of Kuopio

Reviewers:
Professor Pascal Laugier, Ph.D.
Laboratoire d'Imagerie Parametrique
University of Paris

Associate Professor Yongping Zheng, Ph.D.
Department of Health Technology and Informatics
The Hong Kong Polytechnic University

Opponent:
Professor Timo Jämsä, Ph.D.
Department of Medical Technology
University of Oulu

ISBN 978-951-27-0683-9
ISBN 978-951-27-0458-3 (PDF)
ISSN 1235-0486

Kopijyvä
Kuopio 2007
Finland

Saarakkala, Simo. Pre-Clinical Ultrasound Diagnostics of Articular Cartilage and Subchondral Bone. Kuopio University Publications C. Natural and Environmental Sciences 205. 2007. 96 p.
ISBN 978-951-27-0683-9
ISBN 978-951-27-0458-3 (PDF)
ISSN 1235-0486

ABSTRACT

In the modern society, osteoarthrosis (OA) is the most common joint disease with significant sociological and economical impact. OA is characterized by the progressive degeneration of the structure and function of articular cartilage and subchondral bone. Current diagnostic techniques of OA can only detect late-stage changes. The rapid progress in surgical techniques to repair local cartilage lesions has also augmented the need for accurate monitoring of cartilage healing.

Quantitative ultrasound techniques have been developed to permit a characterization of articular cartilage. Previously, an ultrasound indentation instrument was shown to be able to distinguish *in vitro* normal tissue from enzymatically degraded cartilage tissue. Subsequently, quantitative ultrasound imaging (QUI) was demonstrated to be suitable for diagnosing the cartilage surface degeneration as well as the parallel changes in the cartilage-bone interface.

In the present thesis work, the ability of an ultrasound indentation instrument to distinguish different histological degenerative grades of bovine articular cartilage during a spontaneous degeneration process was investigated *in vitro*. Furthermore, the suitability of QUI for detecting mechanically induced, enzymatically induced, or spontaneously developing degenerative changes was investigated. Ultrasound reflection from the articular surface as well as from the cartilage-bone interface were quantified and compared with the histological, biomechanical and biochemical reference measurements. Furthermore, a novel approach for quantifying the cartilage surface roughness from 2D ultrasound images was devised in this thesis work.

A significant linear correlation ($r = 0.883$) was observed between the dynamic modulus, measured with the ultrasound indentation instrument, and the reference modulus from bovine articular cartilage ($n = 70$). Furthermore, the instrument sensitively distinguished histologically normal cartilage from spontaneously degenerated tissue. QUI detected sensitively experimentally induced or spontaneously developing degenerative changes before these characteristic OA alterations could be visualized. The ultrasound roughness index (URI) was demonstrated to be sensitive and specific for histologically confirmed surface fibrillation of articular cartilage tissue. Ultrasound reflection from the cartilage-bone interface increased statistically significantly during the progression of tissue degeneration. All quantitative ultrasound parameters exhibited moderate or good reproducibilities.

These present results indicate that quantitative mechano-acoustic measurements are a feasible way to sensitively characterize articular cartilage. The ultrasound indentation technique was capable of determining short-term mechanical properties of cartilage. The instrument has now been validated; the next stage will be its further development for clinical use. One major benefit of QUI, as compared to more localized measurement techniques, is the possibility to obtain information rapidly from larger areas of articular surfaces as well as from underneath the cartilage surface. QUI techniques could be applied *in vivo* by developing an arthroscopic imaging probe.

Universal Decimal Classification: 534-8, 534.7, 534.8, 681.88
National Library of Medicine Classification: QT 34, QT 36, WE 26, WE 300, WE 348, WN 208
Medical Subject Headings: osteoarthritis/diagnosis; cartilage; cartilage, articular/ultrasonography; collagen; proteoglycans; biomechanics; acoustics; ultrasonics; ultrasonography; numerical analysis, computer-assisted

To my love, Kirsi

ACKNOWLEDGMENTS

This study was carried out during the years 2001-2006 in the Departments of Anatomy and Physics, University of Kuopio, in the Department of Clinical Physiology and Nuclear Medicine, Kuopio University Hospital, and in the Department of Nuclear Medicine, Mikkeli Central Hospital.

I owe my deepest gratitude to my principal supervisor, Professor Jukka Jurvelin, Ph.D., for his professional and inspiring guidance during the whole project. Accomplishing this thesis in the Biophysics of Bone and Cartilage (BBC) -group under his continuous support, optimism and constructive criticism has been a privilege to me.

I express my sincere thanks to my other supervisor, Docent Juha Töyräs, Ph.D., for his extensive collaboration, practical supervision and criticism. His exhaustive enthusiasm and true devotion to science have influenced me much.

I am very grateful to my third supervisor, Professor Heikki Helminen, M.D., Ph.D., for giving me ”fatherly” guidance during the project. Besides supervision, he has placed the resources of the Department of Anatomy at my disposal in the beginning of this project.

I am grateful to official reviewers, Professor Pascal Laugier, Ph.D., and Associate Professor Yongping Zheng, Ph.D., for their constructive criticism to improve this thesis. I give my cordial thanks to Ewen Macdonald, Department of Pharmacology and Toxicology, for revising the language of the thesis.

I send many thanks to all members of the BBC-group for their friendly, helpful and cheerful attitude. Especially, I am deeply indebted to Mikko Laasanen, Ph.D., for his co-operation since the very beginning of our research projects. It has really been a pleasure to work with him - his sense of humour encountered mine even after long measurement days. Further, Jani Hirvonen, B.Eng., M.Sc., is cordially acknowledged for extensive LabVIEW software programming for my studies. I want to express my special thanks also to Rami Korhonen, Ph.D., for conducting numerical analysis and introducing me the ”world of cartilage modeling”. I want to thank Jarno Rieppo, M.D., for the FT-IRIS and histological analyses and valuable discussions. I give thanks to Heikki Nieminen, M.Sc., for constructive criticism and fruitful discussions of ultrasonics during the project. I thank Docent Miika Nieminen, Ph.D., Mikko Hakulinen, Ph.D., and Mikko Nissi, M.Sc., for valuable discussions and support.

I express my gratitude to all of the personnel of the Department of Anatomy. Especially, Mrs. Eija Rahunen, Mrs. Elma Sorsa and Mr. Kari Kotikumpu are acknowledged for their help with the sample processing and laboratory techniques. I want to thank Docent Mikko Lammi, Ph.D., and Kari Törrönen, M.Sc., for conducting the biochemical analyses. Alpo Pelttari, M.Sc., is warmly acknowledged for his technical assistance in SEM imaging. My thanks belong also to Mrs. Arja Hoffren and Mrs. Irma Pääkkönen for the help with the university administration.

I wish to thank the whole personnel of the Department of Physics. My special thanks go to the head of the Department, Professor Jari Kaipio, Ph.D., for valuable discussions and follow-up during my thesis work. Professor Reijo Lappalainen, Ph.D. is acknowledged for collaboration, constructive criticism and discussions.

I wish to thank many members of the personnel of Mikkeli Central Hospital. I am especially grateful to Docent Jari Heikkinen, Ph.D., for giving me the possibility to conduct the thesis work during my hospital specialization period. I also thank Juhani Koski, M.D., Ph.D., for valuable discussions and co-operation in osteoarthitis research.

I want to thank Atria Lihakunta Oyj, Kuopio, and its personnel for the continuous possibility to use bovine knee joints as our research material.

I send my dearest thanks to my parents, Liisa and Lasse Saarakkala, and my brother, Seppo Saarakkala, for their endless encouragement and support during my all studies and whole life.

Finally, I want to express my deepest and dearest thanks to my beloved wife, Kirsi, for her unconditional love and support. Together, we have learnt a lot about the true meaning of life. Her support and understanding have made this thesis possible.

This thesis work was financially supported by several Finnish institutions: the National Technology Agency (TEKES projects 40714/01 and 70061/02), Kuopio University Hospital (EVO grants 5173, 5203 and 5224), the Academy of Finland (projects 47471 and 205886), Etelä-Savo Hospital District (TEVO grant) and National Graduate School of Musculoskeletal Diseases in Finland (TULES). The North Savo Fund of the Finnish Cultural Foundation, The South Savo Fund of the Finnish Cultural Foundation, High Technology Foundation of Eastern Finland, Radiological Society of Finland and Emil Aaltonen Foundation are acknowledged for their highly valuable personal grants.

Kuopio, February 2007

Simo Saarakkala

ABBREVIATIONS

1D	One-dimensional
2D	Two-dimensional
ACR	American College of Rheumatology
B-scan	2D ultrasound image
CC	Amide I absorption (collagen content)
COX	Cyclo-oxygenase
CV	Coefficient of variation
dGEMRIC	Gadolinium Enhanced T1 MRI mapping of cartilage
FE	Finite element
FFT	Fast Fourier Transform
FMC	Medial femoral condyle
FT-IRIS	Fourier transform infrared spectroscopy
GAG	Glycosaminoglycan
LPG	Lateral patello-femoral groove
Mankin score	Cartilage tissue histological degenerative grade
MS	Mankin score
MTP	Medial tibial plateau
MRI	Magnetic resonance imaging
NSAID	Non-steroidal anti-inflammatory drug
OA	Osteoarthrosis
OCT	Optical coherence tomography
PAT	Patella (lateral upper quadrant)
PBS	Phosphate-buffered saline
Rho	Intraclass correlation coefficient
RMS	Root mean square
sCV	Standardized coefficient of variation
SEM	Scanning electron microscopy
SD	Standard deviation
X-ray	Radiographic imaging

SYMBOLS

A	Area of the surface or amplitude of the ultrasound signal
$A_0(z, f)$	Frequency and depth-dependent attenuation function
a	Radius of the indenter (or ultrasound transducer)
α	Attenuation coefficient
c	Speed of sound
C	Compliance
C^{ijkl}	Elastic stiffness matrix
d	Distance
Δf	Frequency bandwidth
E	Young's (elastic) modulus
$E(f)$	Acoustoelectric transfer function
E_{dyn}	Dynamic modulus
E_{DynRef}	Reference dynamic modulus
ϵ	Strain
ϵ_{kl}	Strain tensor
F	Force
f	Frequency
$G(f)$	Acquisition system transfer function
H_a	Aggregate modulus
$H_s(z, f)^2$	Surface-integrated diffraction function
$\mathrm{H_2O}$	Water content
h	Cartilage thickness
I	Intensity of the ultrasound signal
IRC	Integrated reflection coefficient (for the cartilage surface)
IRC_{bone}	Integrated reflection coefficient (for the cartilage-bone interface)
$J(t)$	Creep compliance
k	Permeability or wave number
k_{creep}	Creep rate
$\kappa(a/h, \nu)$	Theoretical scaling factor (indentation geometry)
L	Thickness or measurement length
λ	Wavelength
m	Number of 1D ultrasound scan lines
n	Number of samples or data points
ν	Poisson's ratio
ω	Angular temporal frequency
P	Ultrasound signal power
p	Statistical significance or acoustic pressure
Q_g	Ultrasound signal amplifying-correction factor
R	Ultrasound reflection coefficient (for the cartilage surface)

R_{bone}	Ultrasound reflection coefficient (for the cartilage-bone interface)
R_a	Average surface roughness
R_q	RMS surface roughness
R_c	Ultrasound reflection coefficient for the cartilage surface in the time domain
$R_c^{dB}(f)$	Energy reflection coefficient for the cartilage surface in the frequency domain
r	Pearson's correlation coefficient
r_s	Spearman's correlation coefficient
ρ	Density
S_0	Unprocessed ultrasound signal
S_H	Hamming windowed ultrasound signal
$S_c(z, f)$	Frequency domain ultrasound signal from the cartilage surface
$S_r(z, f)$	Frequency domain ultrasound signal from the perfect reflector
σ	Stress
σ^{ij}	Stress tensor
T	Ultrasound transmission coefficient or length of time window
t	Time
u	Particle displacement
URI	Ultrasound roughness index (for the cartilage surface)
v	Ultrasonic wave velocity
x	Distance
$y(x)$	1D surface profile
Z	Acoustic impedance
z	Distance or depth
$\langle ... \rangle$	Spatial average

LIST OF ORIGINAL PUBLICATIONS

This thesis is based on the following original articles, which are referred to in the text by their Roman numerals (I-V):

I Saarakkala S, Laasanen MS, Jurvelin JS, Törrönen K, Lammi MJ, Lappalainen R, Töyräs J. Ultrasound indentation of normal and spontaneously degenerated bovine articular cartilage.
Osteoarthritis and Cartilage 11: 697-705, 2003.

II Saarakkala S, Korhonen RK, Laasanen MS, Töyräs J, Rieppo J, Jurvelin JS. Mechano-acoustic determination of Young's modulus of articular cartilage.
Biorheology 41: 167-179, 2004.

III Saarakkala S, Töyräs J, Hirvonen J, Laasanen MS, Lappalainen R, Jurvelin JS. Ultrasonic quantitation of superficial degradation of articular cartilage.
Ultrasound in Medicine and Biology 30: 783-792, 2004.

IV Laasanen MS, Saarakkala S, Töyräs J, Rieppo J, Jurvelin JS. Site-specific ultrasound reflection properties and superficial collagen content of bovine knee articular cartilage.
Physics in Medicine and Biology 50: 3221-3233, 2005.

V Saarakkala S, Laasanen MS, Jurvelin JS, Töyräs J. Quantitative ultrasound imaging detects degenerative changes in articular cartilage surface and subchondral bone.
Physics in Medicine and Biology 51: 5333-5346, 2006.

The original articles have been reproduced with permission of the copyright holders.

Contents

1 Introduction 13

2 Structure and composition of articular cartilage 17

3 Osteoarthrosis 19
- 3.1 Background . . . 19
- 3.2 Progress of osteoarthrosis . . . 20
- 3.3 Treatment of osteoarthrosis . . . 21
- 3.4 Diagnostics of osteoarthrosis . . . 23
  - 3.4.1 Clinical diagnostic techniques . . . 23
  - 3.4.2 Pre-clinical diagnostic techniques . . . 24

4 Mechanical characteristics of articular cartilage 29
- 4.1 Background . . . 29
- 4.2 Measurement techniques . . . 29
- 4.3 Theoretical models for mechanical behaviour of articular cartilage . . . 32
  - 4.3.1 Single phasic elastic model . . . 32
  - 4.3.2 Biphasic model . . . 32
  - 4.3.3 Extensions of biphasic model . . . 33

5 Basic physics of ultrasound 35
- 5.1 Ultrasonic waves . . . 35
- 5.2 Generation of medical ultrasonic images . . . 38

6 Ultrasonics of articular cartilage 41
- 6.1 Ultrasound measurement techniques . . . 41
- 6.2 Ultrasound reflection from the cartilage surface . . . 42
- 6.3 Acoustic properties of articular cartilage . . . 45

7 Surface roughness of articular cartilage 49
- 7.1 Surface roughness parameters . . . 49
- 7.2 Ultrasound determination of articular surface roughness . . . 50
- 7.3 Values of articular surface roughness . . . 51

8 Aims of the present study 53

9 Materials and Methods 55
- 9.1 Articular cartilage samples and processing protocols . . . 55
  - 9.1.1 Enzymatically degraded samples . . . 56
  - 9.1.2 Mechanically degraded samples . . . 57
  - 9.1.3 Spontaneously degenerated samples . . . 58
  - 9.1.4 Intact samples from bovine knee joint . . . 58
- 9.2 Ultrasound indentation instrument . . . 59
  - 9.2.1 Experimental measurements . . . 59
  - 9.2.2 Finite element modeling . . . 60
- 9.3 Quantitative ultrasound imaging . . . 60
  - 9.3.1 Ultrasound reflection parameters . . . 61
  - 9.3.2 Ultrasound Roughness Index . . . 62
- 9.4 Reference methods . . . 63

9.4.1 Mechano-acoustic measurements 63
9.4.2 Histological and biochemical analyses 64
9.4.3 Scanning electron microscopy (SEM) 64
9.4.4 Fourier transform infrared spectroscopy (FT-IRIS) 65
9.5 Statistical analyses 65

10 Results **67**
10.1 Ultrasound indentation instrument 67
10.1.1 Experimental measurements 67
10.1.2 Finite element modeling 69
10.2 Relation between cartilage mechanical and acoustic properties 70
10.3 Quantitative ultrasound imaging 70
10.3.1 Enzymatically degraded samples 70
10.3.2 Mechanically degraded samples 71
10.3.3 Spontaneously degenerated samples 72
10.3.4 Intact samples from bovine knee joint 74

11 Discussion **77**
11.1 Ultrasound indentation instrument 77
11.2 Relation between cartilage mechanical and acoustic properties 79
11.3 Quantitative ultrasound imaging 79
11.4 Diagnostic potential of quantitative ultrasound techniques 82

12 Summary and conclusions **85**

References **87**

Appendix: Original publications

CHAPTER I

Introduction

Articular cartilage is specialized connective tissue that covers the ends of the bones in the diarthrodial joints. The main functions of articular cartilage are to dissipate contact stresses during joint loading, to contribute to lubrication mechanisms in the joint, and to provide an almost frictionless articulation in a diarthrodial joint [90, 104]. In order to accomplish these tasks, articular cartilage has unique mechanical properties: the tissue is a biphasic material with an anisotropic, unhomogenous and nonlinear behaviour. This complex mechanical behaviour is a result of the specialized composition and structural organization of the tissue. Articular cartilage consists of one cell type, the chondrocyte, and of an extracellular matrix. The interstitial water contributes 70-80 % to the wet weight of cartilage, while the structural macromolecules, *i.e.* collagens, proteoglycans and noncollagenous proteins, make up the remaining 20-30 % [90, 93]. It is widely accepted that collagen fibrils are mainly responsible for the cartilage tensile stiffness and the dynamic compressive stiffness, while proteoglycans are primarily responsible for the time-dependent and equilibrium properties during compression [13, 64, 71].

Osteoarthrosis (OA) is a very common and severe joint disease causing suffering to the patients and a high economical burden to society [37, 132]. OA is characterized by the progressive degeneration of the articular cartilage along with the abnormal growth of the subchondral bone [21, 31]. Specific OA changes in the cartilage tissue include the progressive disruption of the collagen network and proteoglycans and an increased water content [21]. Previous studies have indicated that the superficial tissue layer in particular contributes significantly to the normal mechanical behaviour of the cartilage [43, 66] and, therefore, degenerative changes in this layer are believed to be highly deleterious to the joint function. In addition to changes in the cartilage tissue, thickening of the subchondral bone, *i.e.* sclerosis, and ostephyte formation are involved in OA [21, 31]. These degenerative changes lead to a decrease in cartilage stiffness [8, 59] impairing the mechanical function of cartilage in the joint. The clinical symptoms of OA include pain, limited mobility and joint deformity.

Currently, OA is diagnosed with radiography (X-ray), followed by magnetic resonance imaging (MRI) or arthroscopy when necessary. Unfortunately, these diagnostic techniques can only detect major OA changes *i.e.* typically near the endpoint of the disease. Visual evaluation and subjective palpation of articular surface during arthroscopy have also been claimed to be unsuitable indicators of early degeneration [8, 30]. Today, there is increased interest in surgical cartilage repair after local cartilage injuries but these techniques need more sensitive evaluation methods of cartilage properties [73].

During the past few years, numerous quantitative techniques have been introduced for the diagnosis of cartilage quality [7, 22, 28, 30, 34, 41, 45, 47, 81, 95, 121]. Most of these techniques are still in the preclinical stage. Clinically, it is important that a diagnostic technique is able to differentiate between the different stages of degeneration but it also needs to be simple to perform and to give reproducible results.

In a recent study, the prototype of an ultrasound indentation instrument was introduced for the diagnosis of cartilage degeneration [70]. The instrument distinguished sensitively between normal and enzymatically degraded cartilage *in vitro* [70], and detected site-dependant variation of cartilage properties in the bovine knee joint *in situ* [69]. In spontaneously degenerating cartilage, however, tissue changes are not as specific as those seen after enzymatic degradation, thus the instrument needs to be capable of detecting these natural degenerative alterations. In this thesis (Study I), the ability of an ultrasound indentation instrument to distinguish different histological degenerative stages of bovine articular cartilage during spontaneous degeneration process was investigated *in vitro*. Furthermore, the results of earlier studies [69, 70] were combined (Study II) with the results of obtained in Study I. The ability of the ultrasound indentation instrument for detecting dynamic stiffness accurately in heterogenous sample population was investigated.

Quantitative ultrasound measurements have been demonstrated to be suitable for the diagnostics of cartilage surface degeneration [28, 34, 45, 61, 72, 73, 114, 119]. Furthermore, it has been proposed that ultrasound reflection from the subchondral bone would increase in OA due to bone sclerosis [50, 114]. In this thesis work, the suitability of quantitative 2D ultrasound imaging was investigated to detect mechanically induced, enzymatically induced, or spontaneously developed degenerative changes (Studies III-V). Ultrasound reflections from the articular surface, as well as from the cartilage-bone interface, were quantified and related to histological, biomechanical and biochemical reference measurements.

In addition to ultrasound reflection from the cartilage surface, cartilage surface roughness can also serve as an index of cartilage degeneration [4, 27, 38, 48]. Unfortunately, most of the cited methods are applicable only under laboratory conditions, and no quantitative technique capable of measuring the articular surface roughness *in vivo* has been described. This study attempted to investigate a novel approach for quantifying the cartilage surface roughness from 2D ultrasound images (Study III). The new method was tested with normal, mechanically, enzymatically or spontaneously degenerated cartilage samples (Studies III-V). The main goal is to devise a roughness parameter which can also be used *in vivo*.

Chapter II

Structure and composition of articular cartilage

"Articular cartilage was made for the purpose of providing a cushion between hard bone and the soft members, so that the latter should not be injured when exposed to a blow or fall, or compression... In the case of joints, it prevents the tissues from being torn by the hard bone." [16]. This citation from the Persian physician Avicenna (980-1037) reveals that the main function of the articular cartilage in the joint was, in general terms, recognized over a thousand years ago. In this chapter, the current knowledge of the cartilage composition and structure is briefly reviewed.

Articular cartilage is composed of two distinct phases. *Solid phase* (or solid matrix) of the cartilage tissue consists of collagen fibrils, negatively charged proteoglycans and cells, *i.e.* chondrocytes. Articular cartilage is relatively acellular tissue as, in adult tissue, only 2 % of the total cartilage volume is occupied by the chondrocytes. Collagen molecules constitute 60-80 % of the cartilage dry weight or approximately 20 % of the wet weight. The collagen molecules assemble to form small fibrils and larger fibers that vary in organization and dimensions as a function of cartilage depth. The diameter of the cartilage collagen fibrils is approximately 20 nm in the superficial zone and 70-120 nm in the deep zone. The collagen fibrils of the cartilage tissue consist mainly of type II collagen which, by definition, helps make tissue a *hyaline cartilage*. In contrast to the *hyaline cartilage*, *fibrocartilage*, *e.g.*, meniscal cartilage, contains mainly type I collagen. In addition to collagen fibrils, proteoglycan macromolecules constitute 20-40 % of the cartilage dry weight or approximately 5-10 % of the wet weight. The proteoglycan aggrecan is composed of a protein core and numerous glycosaminoglycan (GAG) chains attached to the core. Many aggrecan molecules are further bound to a single hyaluronan chain to form a proteoglycan aggregate. [89, 90, 93, 104]

Fluid phase of the cartilage tissue consists of interstitial water and mobile ions. The water phase constitutes 70-80 % of the cartilage total weight and is an important determinant of the physical properties of the tissue. [12, 90, 93]

The typical thickness of human articular cartilage is only a few millimeters, and the structure of the tissue is highly organized and layered. The basic structure of articular cartilage can be divided into four zones (Figure 2.1), *i.e.* superficial zone, middle zone, deep zone and calcified cartilage. In the superficial zone (approximately 10 % of the cartilage thickness), the chondrocytes are flattened and aligned in parallel to the surface. In this region the collagen fibrils are relatively thin and run parallel to each other and the articular surface. The proteoglycan content is at its lowest and the water content is at its highest. In the middle zone, the collagen fibrils have a larger diameter and are oriented randomly. Here the cell density and water content is lower and proteoglycan content is higher than in the superficial zone. In the deep zone, the diameter of the collagen fibrils is at its largest, and the collagen fibrils are oriented roughly perpendicularly to the articular surface. The cell density and water content are at their lowest, the proteoglycan content at its highest but the collagen content is variable in the deep zone. The calcified zone, located between the deep zone and the subchondral bone, joins the cartilage tissue to the subchondral bone. Here the chondrocytes usually express a hypertrophic phenotype. [12, 89, 90, 104]

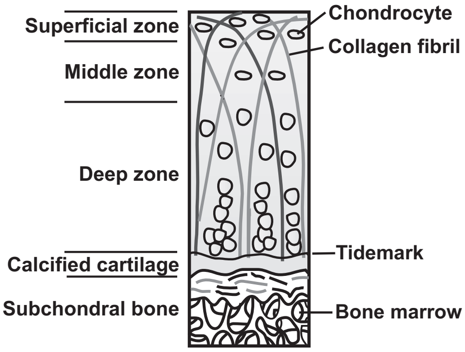

Figure 2.1: Zonal arrangement of cartilage tissue. Tissue can be divided into four zones according to the structure and composition. The subchondral bone is located underneath the cartilage tissue.

Chapter III

Osteoarthrosis

3.1 Background

Osteoarthrosis (OA), also referred to as degenerative joint disease, degenerative osteoarthritis, osteoarthritis or hypertrophic osteoarthritis, is the most common joint disease and it has significant health, sociological and economical impact [132]. It has been estimated that approximately 59 million people will be affected by degenerative joint diseases by the year 2020 in the United States [37].

OA can be regarded as a physiologic imbalance, *i.e.* a "joint failure" similar to "heart failure", in which mechanical factors play a role [110]. Age is the greatest risk factor for OA and, consequently, OA is typically a disorder of elderly people. OA occurs normally in the foot, knee, hip, spine and hand joints. Clinical symptoms of OA include pain, restriction of motion, crepitation with motion, joint effusions and deformity [21]. Inflammatory episodes are frequently encountered in OA and, therefore, the disease is often called *osteoarthritis*. However, primary OA can develop without any known cause. Secondary OA can develop, *e.g.*, after joint or ligament injury, after infection or in a variety of hereditary, metabolic and neurological disorders [21].

It is known that collagen damage, leading to fibrillation of the articular surface, is more harmful to the tissue than the proteoglycan depletion since in mature human cartilage, the turnover time of collagen has been estimated to be more than one hundred years [125]. These degenerative changes lead to a decrease in cartilage stiffness, impairing the ability of the tissue to cope with the high mechanical demands placed on the joint [8, 59]. In addition to changes in the cartilage tissue, specific osteoarthrotic alterations in the subchondral bone include remodeling, thickening (sclerosis), cyst formation and osteophyte formation [21, 31].

It was suggested as early as the 1960's that changes in bone remodeling could precipitate degeneration of cartilage tissue [14]. In 1986, Radin *et al.* proposed that alterations of the subchondral bone, *i.e.* increased bone mass and sclerosis, would occur before deterioration of cartilage structure and properties [110]. The assumption behind the hypothesis was that the mechanical progression of cartilage lesions requires, initially, a stiffening of the subchondral bone. In such situations, transverse stresses at the base of the articular cartilage could cause deep horizontal splits in the tissue [110]. Today it is still not known whether changes in the subchondral bone precede cartilage degeneration or vice versa. However, it has become clear that subchondral bone and articular cartilage comprise a unique functional unit and that the operation of this unit is disturbed in OA. Therefore, it is important that diagnostics and treatment methods of OA should not concentrate solely on the cartilage tissue, but also on the subchondral bone [14].

Unfortunately, no cure for OA exists although much effort has been devoted to this research all over the world. In the following sections, the progression of OA as well as the current treatment and diagnostic options are briefly reviewed.

3.2 Progress of osteoarthrosis

According to Buckwalter and Mankin (1997), the progression of OA can be divided into three phases [21]:

1. *Early degeneration*: There is an increase in the cartilage water content [85] and a decline in proteoglycan aggregation. Simultaneously, alterations in the collagen fibril network, *i.e.* changes in the relative amounts of the minor collagens and the collagen fibrils, can be observed. These changes weaken the integrity of the collagen network matrix and, consequently, lead to cartilage swelling and increased water content. Hence, tissue permeability increases, allowing free water flow in and out of the tissue. All of these changes together debilitate the mechanical performance of articular cartilage by decreasing its mechanical stiffness. It is noteworthy that in this stage, the cartilage surface is frequently still glossy, and no visible surface fibrillation can be seen. In the subchondral bone, an increased density, cyst-like bone cavities or thickening can be observed.

2. *Advanced degeneration*: This stage begins when tissue chondrocytes detect the tissue damage or changes in osmolarity and charge. After the detection of the damage, mediators are released into the tissue by chondrocytes, initiating the cartilage repair process. The repair process involves an increased synthesis of matrix macromolecules and cell proliferation and can last for years. In this stage, the cartilage surface loses its visually glossy appearance and may become discoloured. Furthermore, surface fibrillation and superficial or deep defects reaching the subchondral bone can be observed. Subchondral bone thickening continues and bone cavities are more frequent at this stage.

3. *Late degeneration*: The final stage of OA begins when the chondrocytic response fails to restore cartilage and, consequently, cartilage tissue can be almost completely worn out. The loss of articular cartilage causes severe pain and the other typical clinical symptoms of OA. In this stage, the subchondral bone can be vastly thickened and very dense. The shape of the articulating bone ends may change due to the abrasion induced by the loss of the overlying articular cartilage.

3.3 Treatment of osteoarthrosis

Non-invasive treatment

The clinical conservative treatment is mainly focused on pain reduction, maintaining or improving joint mobility and limiting functional impairment. The recommendations, published by the American College of Rheumatology (ACR), state that the non-pharmacologic treatment (including patient education, physical therapy, weight loss, exercise or assisting devices) should be the initial choice, followed by oral medication for pain relief, if needed [1, 101]. The oral medications initially includes non-steroidal anti-inflammatory drugs (NSAIDs, *e.g.* ibuprofen) and, subsequently, if their response is inadequate, cyclo-oxygenase (COX)-2-selective inhibitors [1, 101]. However, it has been demonstrated that NSAIDs as well as COX-2-inhibitors may have serious adverse effects, especially with long-term use and this must be balanced against the benefits of these oral medications [101].

It has been proposed that glucosamine sulfate could be a safer and more effective oral medication for treatment of OA [51]. Glucosamine sulfate is a slow-acting drug, as compared to traditional NSAIDs, and it is usually delivered orally. Glucosamine is believed to play a part in the repair and maintenance of cartilage tissue. It stimulates cartilage cells to produce GAGs and proteoglycans and, thus, helps tissue to recover from the proteoglycan depletion occuring in OA [51]. In 2001, James *et al.* performed a large literature review of clinical studies that focused on the efficacy of glucosamine sulfate in the treatment of OA [51]. A significant reduction in knee pain, an improved range of motion and a decreased swelling were reported when glucosamine sulfate was compared to placebo. From these data, James *et al.* (2001) concluded that [51]: *"Glucosamine sulfate appears to slow the process of articular degeneration and facilitate the recovery of normal joint mobility."* However, conflicting results have been also published. Lammi *et al.* (2004) and Qu *et al.* (2006) concluded, based on biochemical *in vitro* experiments with bovine normal and osteoarthritic cartilage tissue, that glucosamine sulphate did not increase proteoglycan synthesis in bovine primary chondrocytes [76, 107]. *"Our results raise questions how orally administered glucosamine can manifest its suggested effects on articular cartilage."* [107]. Thus, an unequivocal assessment of the benefits of glucosamine sulfate remains to be done.

Several available treatment methods concentrate exclusively on the cartilage tissue. Very recently, *calcitonin* has been introduced for the treatment of OA [57]. Calcitonin has long been known to inhibit bone resorption but now it has also been hypothesized, based on *in vitro* and *in vivo* results, to have a direct chondroprotective effect on the cartilage [57]. As described earlier, subchondral bone and articular cartilage comprise a unique functional unit and, therefore, this kind of drug may represent an effective treatment attacking both cartilage and subchondral bone metabolic imbalances [57]. However, more randomized clinical studies are needed to support that hypothesis.

Invasive treatment

One potential minimally invasive treatment option is an intra-articular hyaluronan injection. The hyaluronan is a typical polysaccharide found normally in the extracellular matrix in soft connective tissues [101]. In knee OA, both synovial fluid viscosity and hyaluronan concentration are reduced, and hyaluronan injections have been thought to act as fluid replacement [101]. Clinically, a significant reduction of pain and improvement in joint function with few adverse effects have been reported for knee OA. Recently, ACR guidelines were also updated to include hyaluronan injections as an option for OA treatment [1, 101].

Traditional, and probably the most common, invasive methods for treating painful joint conditions in OA are lavage and debridement [49]. Both methods can be conducted during arthroscopy. In lavage, a solution of sodium chloride is injected into the patient's joint. Over 10 liters of fluid can be used in the procedure [88]. In debridement, the rough articular surfaces are shaved, loose debris is removed, all torn or degenerated meniscal fragments are trimmed, and the remaining meniscus is smoothed to a firm and stable rim [88]. In clinical studies, approximately 50 % of treated patients report relief from pain after these arthroscopic procedures [88]. However, there is still much doubt about the true efficacy of these methods [32]. It has been even reported that pain relief in knee OA is no better after arthroscopic lavage or arthroscopic debridement than after a placebo procedure [88]. This is an interesting result since in the United States, the annual cost of these arthroscopic procedures amounts to approximately 3.25 billion dollars [88]. Nonetheless, it was claimed in a very recent study that carefully selected patients may still benefit for arthroscopic debridement [120].

When OA reaches the end-stage, the most common treatment is the installation of an endoprosthesis. When cartilage defects are confined to a small localized area, surgical cartilage repair techniques may offer treatment approach. Usually, these localized cartilage injuries occur after joint trauma. Cartilage repair techniques can be divided into two types: *intrinsic* and *extrinsic* [49]. In the intrinsic type, the cartilage tissue is stimulated to heal via its own spontaneous repair mechanisms. In the extrinsic techniques, active biological compounds are installed in the cartilage defect in order to induce tissue regeneration. Mosaicplasy and autologous chondrocyte transplantation are the most common extrinsic cartilage repair techniques [49]. For a more detailed description of the current status and prospects of cartilage repair techniques, the reader is recommended to read the review by Hunziker (2002) [49].

3.4 Diagnostics of osteoarthrosis

3.4.1 Clinical diagnostic techniques

Clinical examination and X-ray imaging
The basis of OA diagnostics, as in most diseases, is clinical examination. In the examination, the joint is palpated and pain, restriction of joint motion, crepitation with joint motion, joint effusion and joint deformity are evaluated. The clinical examination is usually followed by a radiographic (X-ray) examination (Figure 3.1). Joint space narrowing, a result of the cartilage wear and subchondral bone sclerosis, is a typical sign of the advanced or late stages. Since the water content of the cartilage tissue can be as much as 80 % of the total weight, cartilage tissue does not significantly attenuate X-rays. Therefore, it is not possible to evaluate the status of cartilage tissue from native radiographic images. Thus, the early stage of the disease cannot be visualized in X-ray images.

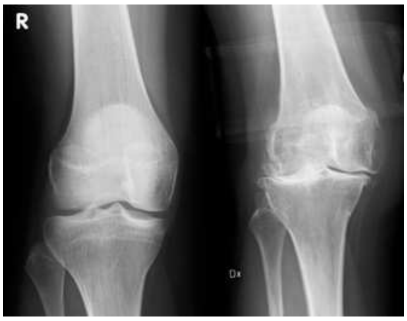

Figure 3.1: X-ray images (ap/pa) of a healthy knee joint (left) and an osteoarthrotic knee joint (right). Typical advanced or late stage changes can be observed in the right-hand image, *i.e.* joint space narrowing and subchondral bone sclerosis.

Arthroscopy
Other common method used in OA diagnostics is arthroscopy in which an arthroscope is inserted into the joint through a hole. Simultaneously, various surgical instruments can be guided into the joint through the other portal. Cartilage integrity, surface fibrillation, defects of the surface, joint ligaments *etc.* can be visually evaluated through the arthroscope. Furthermore, cartilage stiffness is normally evaluated

by manually palpating the articular surface with a blunt probe. Currently, it is not possible to evaluate the cartilage internal structure and the subchondral bone during routine arthroscopy. Despite being current clinical practice, visual evaluation and subjective palpation of the articular surface during arthroscopy are claimed to be insufficient indicators of early degeneration [8, 30]. Clearly, these methods are subjective and significantly dependent on the evaluator [20].

MRI imaging

Magnetic resonance imaging (MRI) is the most promising non-invasive method for OA diagnostics [22]. In routine MRI, thinning and irregularity of cartilage tissue, as well as subchondral bone changes, can be qualitatively evaluated during OA. Recently, Gadolinium enhanced T1 MRI mapping of the cartilage (dGEMRIC) has been suggested to be able to detect the cartilage proteoglycan concentration and distribution [22, 23, 98], also *in vivo* [15]. T2 mapping with MRI has been suggested to be a sensitive way to measure the cartilage tissue collagen content, the orientation of the collagen fibrils as well as the collagen integrity [22, 99, 100, 130]. Recently, it has been reported that both dGEMRIC and T2 mapping predict indirectly mechanical stiffness of the human cartilage *in vitro* [67, 115]. It has also been proposed that the relationship between T2 values and cartilage dynamic stiffness is significant at the clinical field strength (1.5 T) [75]. However, it was alleged in a very recent study that clinical use of T2 mapping is not possible due to many competing factors affecting T2 measurements [23]. The main weakness of MRI imaging is its limited resolution and only the moderate relation between cartilage mechanical stiffness and MRI parameters. Thus, MRI evaluates the tissue microstructure and composition but does not directly measure the mechanical competence of the articular cartilage.

3.4.2 Pre-clinical diagnostic techniques

Indentation measurements

Traditionally, the mechanical performance of the articular cartilage has been quantified with *indentation* measurements. In this technique, the cartilage surface is compressed with a cylindrical or spherical indenter to a predefined strain. Consequently, the force by which the cartilage resists the induced deformation is measured and used as an indicator of cartilage stiffness. Several indentation instruments have been introduced for arthroscopic measurements of cartilage stiffness [7, 10, 30, 81, 95]. With these instruments, however, it is not possible to determine tissue thickness and this is a factor that affects the indentation results, especially with thin cartilage [46, 83, 133].

Ultrasound indentation

To overcome the limitation of unknown cartilage thickness, a technique called *ultrasound indentation* has been introduced for the determination of cartilage mechanical properties. In this technique, the cartilage tissue is compressed with an ultrasound transducer and, simultaneously, the thickness and deformation are calculated from the ultrasound signal reflected from the cartilage-bone interface [58, 70, 121, 134]. Consequently, the material stiffness of tissue can be calculated from the measurements, provided that a realistic mechanical model for cartilage is in use.

In 2002, a handheld ultrasound indentation instrument for the diagnosis of cartilage degeneration was developed in the University of Kuopio [70]. The instrument consists of an unfocused miniature contact ultrasound transducer (diameter = 3.0 mm) mounted on the tip of an arthroscopic indentation instrument (Artscan 200, Artscan Oy, Helsinki, Finland). In the ultrasound indentation technique, cartilage is compressed manually with the ultrasound transducer and the ultrasound signal is collected simultaneously (Figure 3.2A). The resisting force is measured with the strain gauge inside the instrument. Thickness and deformation of the cartilage are detected in real-time from the ultrasound signal. From this information, the cartilage dynamic (instantaneous) modulus can be calculated. Furthermore, manual creep experiments can be conducted with the instrument by inducing and maintaining a constant stress on the cartilage surface and simultaneously measuring the time-dependent change in the strain [70]. In addition to mechanical measurements, ultrasound reflection from the cartilage surface can be determined with the instrument. In order to keep the transducer at a constant distance from the articular surface, a sleeve has been attached over the ultrasound transducer (Figure 3.2B). The echo amplitudes of the reflected sound from the articular surface are measured and normalized with the echo signal from the perfect reflector, *i.e.* from the saline-air interface.

The ultrasound indentation instrument has been demonstrated to be able to distinguish sensitively normal and enzymatically degraded cartilage from each other *in vitro* [70]. Furthermore, the instrument has enabled an objective registration of the site-dependent variation of cartilage properties in the bovine knee joint *in situ* [69]. Typical values for the dynamic modulus, as measured with the instrument, were 3.4-10.0 MPa and 3.0-4.7 MPa for healthy and degenerated tissue, respectively [69, 70]. The creep rate ($k_{creep} = \frac{dJ(t)}{d\ln t}$, where $J(t)$ is the creep compliance and t is time), determined manually in a creep experiment, was typically 21.6-27.8 kPa/s in healthy compared to 29.0-62.0 kPa/s for degenerated tissue [70]. The ultrasound reflection coefficient for the cartilage surface was typically 4.2-5.7 % and 2.3-4.8 % for healthy and degenerated tissue, respectively [69, 70].

Optical coherence tomography

Recently a novel imaging modality, optical coherence tomography (OCT) was in-

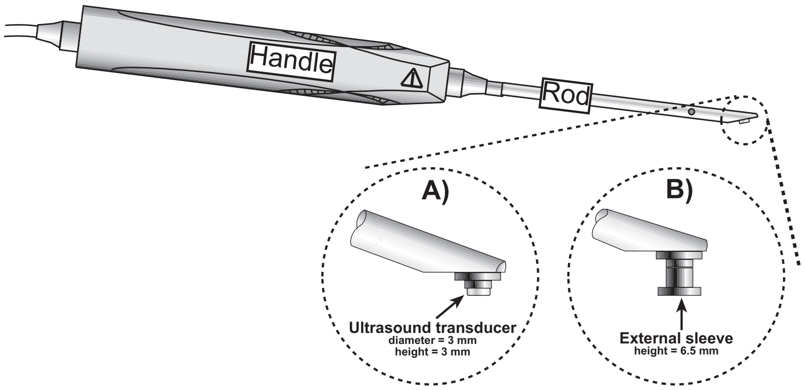

Figure 3.2: A) Schematic presentation of the indentation geometry of the ultrasound indentation instrument [70]. B) Ultrasound reflection from the cartilage surface is also quantified with the instrument by attaching a plastic sleeve over the ultrasound transducer.

troduced for the assessment of articular cartilage microstructure [47]. The physical background of OCT is somewhat analogous to ultrasound - OCT measures reflection of infrared light instead of sound. The resolution of OCT is very high, being typically in the range of 10-20 micrometers [102]. OCT imaging has been demonstrated to be capable of measuring cartilage thickness [112], collagen network organization [35] as well as other histologically confirmed structural changes [3, 80]. In addition to *in vitro* studies, OCT has been tested arthroscopically *in vivo* with porcine [102] and rat [3] articular cartilage, and with human cartilage during open knee surgery [80]. There is one main limitation of cartilage OCT imaging, and in that way it is similar to MRI, *i.e.* it provides information on tissue microstructure but not directly on the cartilage mechanical properties. Furthermore, the penetration of light in the cartilage is limited.

Electromechanical measurements

Novel electromechanical diagnostic methods have been tested in pre-clinical investigations [41, 79, 108, 113]. In these techniques, electromechanical properties, such as streaming potentials, of cartilage tissue are measured, in unconfined compression or in indentation geometry, with a mechanical tester coupled with a microelectrode. The technique has been reported to be especially sensitive for detecting the degradation of cartilage proteoglycans [79]. Electromechanical measurements do not provide information about tissue thickness, which could possibly affect the determination of cartilage electromechanical properties. Furthermore, electromechanical measurements do not permit acquisition of high resolution images of the tissue.

High-frequency ultrasound analysis

Various studies have been published to test the suitability of using high-frequency ultrasound in the detection of cartilage degeneration [2, 5, 28, 29, 34, 45, 50, 61, 72, 73, 78, 103, 106, 114, 119, 123, 124]. In this technique, an ultrasound wave pulse is transmitted through the cartilage tissue, and the reflection or backscattering of sound is measured. The ultrasound technique has been demonstrated to be especially sensitive for superficial collagen degeneration. Furthermore, ultrasound measurements offer great potential for direct determination of cartilage surface roughness.

Ultrasound imaging has theoretically greater potential, compared to other techniques, for providing direct information about the mechanical performance of cartilage since the ultrasound is a mechanical wave motion. The main weakness of the ultrasound technique is that it requires at least a minimally invasive approach in clinical use. Some kind of non-invasive ultrasound imaging of articular cartilage could also be an option, although the ultrasound penetration would then be limited to small areas in the joint. More detailed information of the ultrasound technique for the characterizing acoustic properties of cartilage can be found in the chapter "Ultrasonics of articular cartilage".

Chapter IV

Mechanical characteristics of articular cartilage

4.1 Background

In order to accomplish the demanding task of minimizing and dissipating large stresses in the joints, articular cartilage has unique mechanical properties. Cartilage tissue is an inhomogeneous, layered poroelastic material with nonlinear and anisotropic mechanical properties [126]. When an external load is applied onto the joint, cartilage deforms to increase the contact area and to enhance joint congruence. Consequently, a combination of compressive, tensile and shear stresses is generated in cartilage. The response of the tissue can be significantly different for each of these stress types. It is known that the collagen network is mainly responsible for the dynamic compressive and tensile response of the cartilage tissue whereas proteoglycans are mainly responsible for the static compressive stiffness of cartilage [64].

4.2 Measurement techniques

Traditionally, cartilage mechanical properties have been measured in three different measurement configurations [90]: *unconfined compression, confined compression and indentation.* In *unconfined compression*, cartilage tissue (without the subchondral bone) is compressed between two smooth metallic plates, allowing the fluid flow only in the lateral direction (Figure 4.1A). In *confined compression*, a cartilage sample, with or without the subchondral bone, is placed in a chamber and, subsequently, compressed with a porous filter (Figure 4.1B). In this approach the fluid can only flow axially through the tissue surface into the filter. In *indentation*, cartilage is typically compressed with a cylindrical plane-ended or spherical-ended indenter (Figure 4.1C). Fluid flow outside the indenter-cartilage contact is possible in both the lateral and axial directions. As the cartilage tissue is naturally attached to the subchondral bone, *indentation* measurements can be performed *in vivo* while the other configurations are limited to *in vitro* studies.

When cartilage tissue is compressed, a loss of volume occurs since the interstitial fluid flows out from the tissue. This phenomenon is primarily responsible for the time-dependent viscoelastic behaviour of cartilage during compression. The movement of interstitial fluid through the tissue is limited by frictional drag forces between the fluid and the solid matrix and, consequently, high hydrostatic pressures are developed within the matrix [90]. The behaviour of cartilage under constant compressive loading (stress) is called *creep* (Figure 4.2A) and the behaviour under constant compressive displacement (strain) is called *stress-relaxation* (Figure 4.2B). When the tissue reaches its equilibrium state, no fluid flow or pressure gradients exist and, consequently, the entire stress is carried by the solid matrix [90].

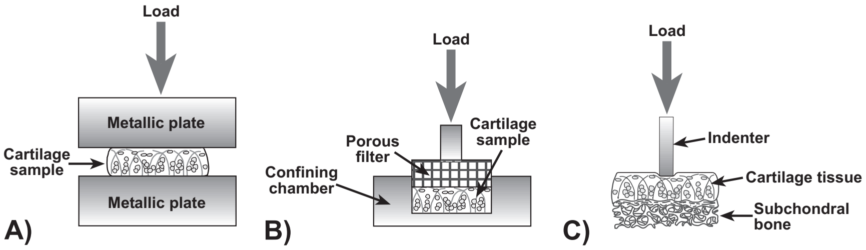

Figure 4.1: Schematic presentation of the typical measurement configurations in use for mechanical testing of the articular cartilage. A) *Unconfined compression*: the tissue is compressed between two smooth metallic plates allowing fluid flow in the lateral direction. B) *Confined compression*: the tissue is placed in a metallic chamber and compressed with a porous filter allowing fluid flow axially through the filter. C) *Indentation*: the tissue is compressed with a cylindrical plane-ended or spherical-ended indenter allowing fluid flow in both lateral and axial directions.

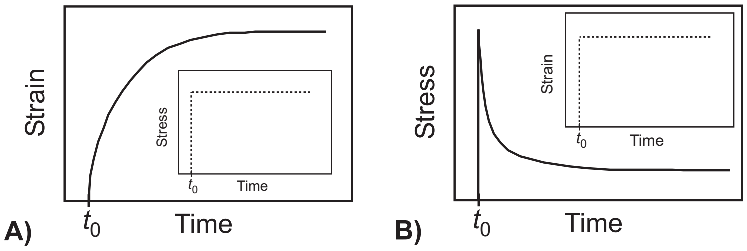

Figure 4.2: A) In a creep measurement, cartilage tissue deformation (strain) is recorded under a constant load (stress) applied at t_0. B) In a stress-relaxation measurement, the cartilage tissue load (stress) is recorded under a constant deformation (strain) applied at t_0.

Table 4.1: Basic equations for the determination of isotropic elastic parameters of cartilage.

Parameter	**Equation**	**Number**
Stress (σ)	$\sigma = \frac{dF}{dA}$	(1)
Strain (ϵ)	$\epsilon = \frac{L'-L}{L}$	(2)
Young's modulus (E) (stress-strain ratio in unconfined compression)	$E = \frac{\sigma_a}{\epsilon_a}$	(3)
Poisson's ratio (ν) (unconfined compression)	$\nu = \frac{\epsilon_l}{\epsilon_a}$	(4)
Shear modulus (μ)	$\mu = \frac{E}{2(1+\nu)}$	(5)
Aggregate modulus (H_A) (stress-strain ratio in confined compression)	$H_A = \frac{1-\nu}{(1+\nu)(1-2\nu)}E$	(6)
Young's modulus (indentation geometry)	$E = \frac{(1-\nu^2)\pi a}{2\kappa h}\frac{\sigma}{\epsilon}$	(7)
Shear modulus (indentation geometry)	$\mu = \frac{(1-\nu)\pi a}{4\kappa h}\frac{\sigma}{\epsilon}$	(8)

Explanation of the symbols:

F	Reaction force
A	Area of the surface in which the force is acting
L	Initial thickness
L'	Thickness after compression
σ_a and ϵ_a	Axial stress and strain
ϵ_l	Lateral strain
a	Indenter radius
h	Cartilage thickness
$\kappa(a/h, \nu)$	Theoretical scaling factor due to finite and variable cartilage thickness [46].

When cartilage is compressed under constant stress (creep measurement) or strain (stress-relaxation measurement), its mechanical properties can be directly determined by measuring the displacement and force as a function of time. At mechanical equilibrium, the measured stress (eq. (1) in Table 4.1) and strain (eq. (2) in Table 4.1) can be used to calculate the elastic (equilibrium) modulus for the tissue.

In unconfined compression geometry, the Young's modulus (E) at equilibrium can be calculated using equation (3) (Table 4.1). Poisson´s ratio (ν) is determined by equation (4) (Table 4.1). In an isotropic elastic material, the shear modulus (μ) is related to the Young's modulus and Poisson's ratio according to equation (5) (Table 4.1).

In confined compression geometry, the elastic modulus can be determined analogously to Young's modulus in unconfined compression. This modulus in confined compression is called the aggregate modulus (H_A), and it can be related to the Young's modulus and Poisson's ratio in elastic and isotropic materials (eq. (6) in Table 4.1).

In indentation geometry, it can be shown, after an elaborate calculation, that the Young's modulus at equilibrium can be derived from equation (7) (Table 4.1). The shear modulus in indentation geometry can be calculated from equation (8) (Table 4.1).

The elastic properties of articular cartilage have been widely characterized in the literature. Young's modulus (E) or aggregate modulus (H_A) values around 0.2-1.5 MPa have been reported for healthy cartilage tissue depending on the measurement geometry used [8, 9, 11, 24, 33, 54, 55, 56, 60, 63, 71, 91, 92, 129]. Equilibrium Poisson's ratio (ν) values for healthy tissue have been reported to be in a range of 0.00 - 0.43 [11, 33, 56, 63]. The instantaneous or dynamic ($t \rightarrow 0$) modulus has been reported to be around 1.5 - 20 MPa [24, 40, 71, 77, 109].

4.3 Theoretical models for mechanical behaviour of articular cartilage

4.3.1 Single phasic elastic model

In a homogeneous elastic material, the mechanical properties are constant within the material, and in an isotropic elastic material, the mechanical properties are uniform in all directions [6]. Otherwise the material is said to be inhomogeneous and anisotropic. The linear relationship between the stress and strain is described by the generalized Hooke's law:

$$\sigma^{ij} = C^{ijkl}\epsilon_{kl}, \tag{4.1}$$

where σ^{ij} is the stress tensor, C^{ijkl} is the elastic stiffness matrix and ϵ_{kl} is the strain tensor. In order to characterize the mechanical behaviour of an anisotropic material altogether 21 stiffness components (elastic constants, C^{ijkl}) are needed. If the material has mutually perpendicular planes of elastic symmetry (orthotropic material), nine elastic constants are needed. If we assume the same properties in one plane (*e.g.* x-y plane) and different properties in the direction normal to this plane (*e.g.* z-axis), the material is called transversely isotropic, and it can be described by five independent elastic constants. Finally, if the material is perfectly isotropic, *i.e.* it has the same elastic properties in all planes, two independent elastic constants are needed: the Young's modulus (E) and Poisson's ratio (ν).

4.3.2 Biphasic model

As articular cartilage is composed of two distinct phases, *i.e.* solid and fluid, the mechanical response of the cartilage tissue to the applied load is time-dependent, *i.e.* the tissue exhibits viscoelastic behaviour. This behaviour is related to the interstitial fluid flow through the porous-permeable solid matrix as well as to the time-dependent viscoelastic deformation of the solid matrix itself [90, 93]. Consequently, a linear single phasic elastic model is inadequate for characterizing time-dependent mechanical behaviour in cartilage. The most traditional model for characterizing the mechanics of articular cartilage, taking the interstitial fluid movement into account, is the linear *isotropic biphasic model* [91]. In the biphasic theory, the solid matrix is assumed to be isotropic, linearly elastic and incompressible. The fluid phase is assumed to be incompressible and inviscid [91]. Consequently, in addition to elastic parameters which can be calculated from equation (4.1), a knowledge of the tissue permeability (k) is needed for characterizing the time-dependent behaviour of the tissue.

The tissue permeability (k) can be determined direcly or indirectly. In the direct determination, the cartilage tissue specimen is positioned under the pressure gradient and the rate of fluid flow through the tissue is measured. In the indirect technique, experimental mechanical measurements are conducted and, subsequently, the theoretical model is fitted to the experimental data. The permeability of the normal articular cartilage is in the order of $10^{-15} - 10^{-16}$ m^4/Ns [90].

The biphasic model indicates that articular cartilage behaves like an equivalent incompressible (ν=0.5) single phasic elastic material during instantaneous loading ($t \to 0$). In an equilibrium state, the Young's modulus (E) (or the shear modulus (μ)) and the Poisson's ratio of the true solid matrix can be determined [83].

4.3.3 Extensions of biphasic model

Cartilage tissue is known to exhibit different responses during compression and tension experiments. Therefore, neither the single phasic elastic theory nor the isotropic biphasic theory provides a comprehensive characterization of cartilage mechanics. Consequently, several more advanced models have been introduced. The most important ones of these models are listed below [128]:

Transversely isotropic model

Transversely isotropic model has six material parameters: Young's modulus (E_1) and Poisson's ratio (ν_{12}) in the transverse plane (parallel to the articular surface), Out-of-plane Young's modulus (E_3) and Poisson's ratio (ν_{31}), Out-of-plane shear modulus (μ_{13}) and permeability (k). Typical values for material parameters are [65]: E_1 = 1-19 MPa, E_3 = 0.46 MPa, ν_{12} = 0.5, ν_{31} = 0, μ_{13} = 0.4-6.3 MPa, $k = 0.2 - 5.0 \times 10^{-15}$ m^4/Ns. The most crucial advantage obtained with this model, as compared to elastic isotropic models, is the inclusion of the response of those collagen fibrils oriented parallel to the surface in the superficial cartilage layer. This is important as it has been demonstrated that the superficial layer significantly contributes to the stiffness of articular cartilage measured in indentation geometry [66]. However, this model still fails to predict the compression-tension nonlinearity of the tissue.

Fibril reinforced model

In the fibril reinforced model, the compression-tension nonlinearity is taken into account by inclusion of the collagen fibril network, running in three mutually orthogonal directions. The collagen network is simulated with the elastic or viscoelastic springs embedded in the isotropic matrix. The material parameters of the fibril reinforced model are Young's modulus (E_m) and Poisson's ratio (ν_m) of the drained porous matrix, permeability (k), and the Young's modulus of the fibril network ($E_f = E_f^{\epsilon}\epsilon_f + E_f^0$, where ϵ_f is tensile srain). Typical values for material parameters are [64]: $E_m = 0.10$ - 0.34 MPa, $\nu_m = 0.42$, $E_f^{\epsilon} = 20$ - 190 MPa, $E_f^0 = 0.10$ - 1.00 MPa and $k = 0.6 - 4.0 \times 10^{-15}$ m^4/Ns. The advantage of the fibril reinforced model, as compared to the transversely isotropic model, is that the fibrils resist only tension. Thus, the compression-tension nonlinearity can be characterized with this model. Furthermore, time-dependent deformation related to intrinsic matrix viscoelasticity can be taken into account [82].

Triphasic theory

Triphasic theory is an extension of the biphasic model but incorporates three phases: an incompressible solid, an incompressible fluid and a monovalent ionic phase [74, 122]. The model assumes that the total stress of the tissue is composed of the fluid stress, solid stress and chemical potentials. This model can be used to faithfully include the effect of cartilage tissue swelling. However, the model, in its current formulation, fails to predict the compression-tension nonlinearity as well as the response of those collagen fibrils oriented parallel to the surface in the superficial cartilage layer.

CHAPTER V

Basic physics of ultrasound

5.1 Ultrasonic waves

Waves in One Dimension

In the following presentation, it is assumed that the material in which the ultrasonic wave is propagating is homogenous, linear and isotropic.

In the ultrasonics of materials, two distinct types of plane waves can be generated: *transverse* and *longitudinal*. In the transverse wave type, a particle moves perpendicularly to the direction of wave propagation. Since the particle motion in transverse waves is associated with shear stress, the transverse wave type is often called a *shear wave*. Shear waves cannot be generated in low-viscosity fluids such as water or air. In the longitudinal wave type, a particle moves parallel to the direction of wave propagation. This wave type is often called a pressure wave or P-wave since the stress of the periodic compression and tension of the particles is along the direction of propagation. [36, 118, 127]

The single particle displacement (u) in a material, in which the ultrasonic wave is propagating, is a function of distance (x) and time (t), *i.e.* $u = u(x, t)$. It can be shown that the particle displacement satisfies the *linear wave equation* [118]:

$$\frac{\partial^2 u}{\partial x^2} - \frac{1}{v^2}\frac{\partial^2 u}{\partial t^2} = 0, \tag{5.1}$$

where v is the phase (wave) velocity. The common solitary wave function satisfying the wave equation is of the following type [118]:

$$u(x, t) = u_0 e^{j(\omega t - kx)}, \tag{5.2}$$

where ω is the angular temporal frequency ($\omega = 2\pi f$, f=frequency) and k is the wavenumber ($k = \frac{2\pi}{\lambda}$, λ=wavelength).

In longitudinal type waves, compressive stress (σ) is associated with the wave motion [118]. In a long, thin rod, the phase velocity of the longitudinal wave in a homogenous isotropic medium (v_l) is related to the Young's modulus (E) and material density (ρ) (eq. (1) in Table 5.1).

In transverse type waves, shear stress is associated with the wave motion [118]. As with longitudinal type waves, it can be presumed that the phase velocity of the transverse wave (v_t) is related to the elastic shear modulus (μ) and material density (ρ) (eq. (2) in Table 5.1).

It can be derived that the acoustic pressure (p), driving the traveling longitudinal type wave in linear elastic material, is related to the Young's modulus and the particle displacement ($\frac{\partial u}{\partial x}$) (eq. (3) in Table 5.1). [118]

Waves in Three Dimensions (bulk waves)

If one assumes that bulk waves travel as a planar wave front in isotropic, homogenous material, the major difference between bulk waves and one dimensional waves will be in the Poisson's effect, *i.e.* the medium is compressed in one direction and simultaneously expanded in other directions. In this kind of situation, the phase velocity of the 3D longitudinal type wave (v_l) can be presented as a function of Young's modulus (E), material density (ρ) and Poisson's ratio (ν) (eq. (4) in Table 5.1). [36, 118, 127]

In contrast to 3D longitudinal type waves, the shear deformation in bulk material causes no new elastic effects, and so the volume does not change. This means that the phase velocity of 3D transverse type waves (v_t) is the same as in the 1D situation (eq. (2) in Table 5.1). [36, 118, 127]

Acoustic impedance and intensity

The acoustic impedance can be shown to be linearly related to the density of the material (ρ) and the longitudinal wave velocity (v_l) (eq. (5) in Table 5.1). A more generalized form of the specific acoustic impedance includes absorption and anisotropic material effects. In this kind of situation, the acoustic impedance can be mathematically expressed as complex variable, $Z = R + iX$ (where R is the real resistive component, X is the reactive component related to absorption and $i = \sqrt{-1}$). At a boundary, the difference in acoustic impedances between two materials defines the amount of ultrasound energy reflected from, or transmitted through, the boundary. [36, 118, 127]

The energy intensity (energy per unit time per unit area) of a longitudinal type wave is proportional to the acoustic pressure and acoustic impedance, as seen in equation (6) (Table 5.1). Hence, for a given acoustic energy, the pressure can be quite large in a material with high acoustic impedance. In experimental ultrasonics, it is often necessary to compare measured ultrasonic signal intensity or pressure amplitude with the reference intensity or amplitude. These differences in intensities (ΔI) or amplitudes (ΔA) are conveniently expressed in a decibel (dB) scale (eqs. (7) and (8) in Table 5.1). [36, 118, 127]

Ultrasonic reflection and refraction

Ultrasonic reflection and refraction deal with the situation when a propagating plane wave arrives at the interface between two materials, *e.g.*, from water to air. If a wave arrives in normal incidence, *i.e.* perpendicular to the interface, from material one to material two, part of the wave is reflected back and part of the wave is transmitted through the interface. This ratio of the incident (i) wave pressure amplitude and reflected (r) or transmitted (t) wave pressure amplitude is characterized by the reflection (R) or transmission (T) coefficients (eqs. (9) and (10) in Table 5.1). It can be shown that the the reflection (R) or transmission (T) coefficients in an isotropic, homogenous medium are dependent on the acoustic impedances around the interface (eqs. (9) and (10) in Table 5.1).

If a wave arrives at an oblique incidence from material 1 to material 2, the transmitted (t) wave is also refracted at the interface according to Snell's law (eq. (11) in Table 5.1). After geometrical calculations, one can derive the pressure reflection and transmission coefficients in that kind of situation (eqs. (12) and (13) in Table 5.1). Equation (9) (Table 5.1) is especially suitable in diagnostic ultrasound when reflected (p_r) and incident (p_i) ultrasound signal pressure amplitudes are measured, and the acoustic impedance of the first medium is known. In that kind of situation, the calculated reflection coefficient is related to the acoustic impedance of the second material and, therefore, also to the mechanical properties of the second material. [36, 118, 127]

Ultrasound attenuation

In an ideal material, the acoustic pressure of a traveling ultrasonic wave remains constant and, hence, the energy is conserved. However, in real materials, the acoustic energy of a traveling wave does not remain constant, *i.e.* an attenuation phenomenon takes place. The attenuation process can be divided into three components: *absorption, scattering* and *beam spreading*. In absorption, the energy of motion is converted into heat energy. In scattering, the energy of motion is diverted from the "main" wave into waves traveling at different directions. In beam spreading, the energy is redistributed over a different area but remains still part of a single wave. Mathematically, attenuation by absorption or scattering of an ultrasonic wave can be represented as a decaying exponential (eq. (14) in Table 5.1). Furthermore, the ultrasound signal attenuation coefficient (α) is significantly dependent on the frequency ($\alpha = bf^d$, where f is the frequency and b and d are experimentally determined coefficients). [36, 118, 127]

Table 5.1: Basic equations for the ultrasonic wave propagation in a material. The numerals one and two refer to the material before and after the acoustic interface, respectively.

Parameter	**Equation**	**Number**
Longitudinal wave velocity in 1D (v_l)	$v_l = \sqrt{\frac{E}{\rho}}$	(1)
Transverse wave velocity in 1D (v_t)	$v_t = \sqrt{\frac{\mu}{\rho}}$	(2)
Acoustic pressure (p)	$p = E\frac{\partial u}{\partial x}$	(3)
Longitudinal wave velocity in 3D (v_l)	$v_l = \sqrt{\frac{E}{\rho}(\frac{1-\nu}{(1+\nu)(1-2\nu)})}$	(4)
Acoustic impedance (Z)	$Z = \rho v_l$	(5)
Intensity (I)	$I = \frac{p^2}{2Z}$	(6)
The difference in ultrasonic signal intensities (ΔI) in decibel-scale	$\Delta I = 10\log\frac{I_1}{I_0}$	(7)
The difference in ultrasonic signal amplitudes (ΔA) in decibel-scale	$\Delta A = 20\log\frac{A_1}{A_0}$	(8)
Reflection coefficient (R) in normal incidence	$R = \frac{p_r}{p_i} = \frac{Z_2-Z_1}{Z_2+Z_1}$	(9)
Transmission coefficient (T) in normal incidence	$T = \frac{p_t}{p_i} = \frac{2Z_2}{Z_2+Z_1}$	(10)
Snell's law	$\frac{\sin\theta_i}{\sin\theta_t} = \frac{v_1}{v_2}$	(11)
Reflection coefficient (R) in oblique incidence	$R = \frac{p_r}{p_i} = \frac{Z_2\cos\theta_i - Z_1\cos\theta_t}{Z_2\cos\theta_i + Z_1\cos\theta_t}$	(12)
Transmission coefficient (T) in oblique incidence	$T = \frac{p_t}{p_i} = \frac{2Z_2\cos\theta_i}{Z_2\cos\theta_i + Z_1\cos\theta_t}$	(13)
Exponential attenuation law	$p(x) = p_0 e^{-\alpha x}$	(14)

The explanation of the symbols:

E	Young's modulus
ρ	Material density
μ	Shear modulus
u	Single particle displacement
x	Distance
ν	Poisson's ratio
v	Ultrasonic wave velocity
p	Acoustic pressure
I_1 and I_0	Ultrasonic signal intensity and reference signal intensity
A_1 and A_0	Ultrasonic signal amplitude and reference signal amplitude
p_r	Pressure amplitude of the reflected ultrasonic wave
p_i	Pressure amplitude of the incident ultrasonic wave
p_t	Pressure amplitude of the transmitted ultrasonic wave
Z_1	Acoustic impedance of the material before the interface
Z_2	Acoustic impedance of the material after the interface
θ_i	Angle between the incident ultrasonic wave and the normal of the interface
θ_t	Angle between the transmitted ultrasonic wave and the normal of the interface
v_1	Ultrasonic wave velocity in the first material before the interface
v_2	Ultrasonic wave velocity in the second material after the interface
$p(x)$	Ultrasonic signal pressure amplitude at a distance x in an attenuating material
p_0	Ultrasonic signal pressure amplitude before attenuating material
α	Pressure amplitude attenuation coefficient

5.2 Generation of medical ultrasonic images

Ultrasonic waves are created (or transduced) from electrical or optical signals by ultrasonic transducers. Transducers can also convert ultrasonic waves back into electrical or optical signals. The most common transducer type is the *piezoelectric transducer*. The principle of this transducer is based on the *direct piezoelectric effect* in which a piezoelectric material responds to a mechanical deformation by developing a charge on its surface. The applied mechanical stress is related to the output voltage (or current). The reverse phenomenon, the *indirect piezoelectric effect* produces a mechanical deformation when the piezoelectric material is subjected to an electric field. Hence, the desired ultrasound pulse can be produced by applying an alternating voltage pulse to the faces of the piezoelectric material. Conversely, if an ultrasonic wave passes through the piezoelectric material, the material contracts and expands producing an alternating electric field, *i.e.* voltage, across the measuring electrodes. More details of the generation of the ultrasound transducers is in the literature, *e.g.*, by Shull and Tittmann (2002) [118].

The most common configuration for transmitting and receiving ultrasound signals in medical ultrasonics is the *pulse-echo method*. In this method, a single transducer acts as the transmitter and the receiver. This method is especially suitable for analysis of materials with limited access to a single side. In most cases, this is the situation in medical ultrasonics.

In medical ultrasonics, phased ultrasonic arrays are commonly used. Every single ultrasound transducer independently transmits and receives the ultrasound signal. The data from each scan line is collected, analyzed and some predetermined value (*e.g.* amplitude or time of flight) is calculated and plotted against position (or depth). When this is repeated in all adjacent scan lines, a 2D ultrasound image is generated. Thus, the typical medical ultrasound 2D image (B-scan) contains the location in a lateral direction plotted in the x-axis, and the location in the axial direction (depth) plotted in the y-axis. In medical devices, the depth of different tissues is determined by measuring the exact time of flight of the ultrasound signal travelling from the transducer to the acoustic interface. The speed of sound is assumed to be constant in human tissues and, subsequently, the depth corresponding to the time of flight can be calculated. It is also possible to generate an ultrasound 2D image by using a single transducer which is moved mechanically by a motor in a lateral direction.

The frequency range of an ultrasound transducer specifies the resolution in the axial direction, *i.e.* a better resolution is achieved with a higher ultrasound frequency. However, tissues attenuate higher frequencies more than lower frequencies limiting the possible scan depth in the tissue. Consequently, in medical ultrasonics, the optimal frequency range depends on the depth of the tissue to be investigated, and it is always a compromise between the axial resolution and scan depth. For instance, a center frequency of 3.5 MHz is used in the abdomenal area, a center frequency of 7 MHz is used for breast imaging, whereas frequencies as high as 30 MHz can be used for skin imaging.

Chapter VI

Ultrasonics of articular cartilage

6.1 Ultrasound measurement techniques

Contact technique

In the contact technique, cartilage tissue is often detached from the subchondral bone and, subsequently, installed between an ultrasound transducer and a metallic plate. Thus, the transducer is in direct contact with the cartilage surface. An ultrasound wave is transmitted through the cartilage and the echoes from the interface between cartilage and metallic plate are recorded. An ultrasound transducer may also be connected to the high-resolution material testing device allowing simultaneous mechanical measurements in unconfined compression geometry (see *e.g.* [96]). Hence, the cartilage sample can be compressed to a predefined strain and the force by which the tissue resists deformation can be measured simultaneously as the ultrasound signal is collected. This configuration is designed for *in vitro* testing. With this set up, the speed of sound and attenuation in the tissue with or without mechanical testing can be determined [96, 123].

The contact technique may also be applied without detaching cartilage from the subchondral bone. In this case, the echoes from the interface between cartilage and subchondral bone are recorded. With this set up, it is possible to determine a value for the ultrasound reflection coefficient for the cartilage-bone interface. Furthermore, the cartilage thickness can be determined by calculating the time of flight and assuming a constant speed of sound. This technique is suitable for *in vivo* testing, and it is applied in ultrasound indentation measurements [58, 70, 121, 134] enabling the determination of mechanical and acoustic properties of tissue.

Non-contact technique

In the non-contact technique, an ultrasound transducer is immersed in a coupling medium, *e.g.*, water or saline solution, and set at a constant distance from the cartilage surface. Thus, an ultrasound wave arrives first at the interface between the coupling medium and the cartilage surface, and part of the wave is reflected back while the rest is transmitted into the tissue. Subsequently, the transmitted wave arrives at the interface between the cartilage and subchondral bone, and is reflected back. Consequently, values for the ultrasound reflection coefficients for the cartilage surface and for the cartilage-bone interface can be determined in the non-contact technique. In addition, the thickness of the cartilage tissue can be calculated from the flight time information between these two acoustic interfaces.

Quantitative ultrasound imaging of the articular surfaces is based on the non-contact method [5, 28, 34, 61, 72, 73, 119]. In addition, an ultrasound indentation instrument, when an external sleeve is attached over the ultrasound transducer [70], utilizes a non-contact method in point-like measurements for ultrasound signal reflection. Zheng *et al.* (2004) applied the non-contact tehnique for investigating the feasibility of ultrasound monitoring for assessing the transient depth-dependent osmotic swelling and solute diffusion in normal and degenerated articular cartilage samples [137].

Other techniques

Other ultrasound measurement techniques have been utilized in the characterization of cartilage mechano-acoustic properties. Zheng *et al.* (2002) measured the depth-dependent equilibrium strains of cartilage tissue under axial compression [135]. In that measurement geometry, ultrasound pulses were transmitted into the cartilage through a thin layer of subchondral bone under the sample [135]. The same authors used a similar geometry for mapping the transient interstitial displacements of full-thickness cartilage samples *in situ* [136]. Fortin *et al.* (2003) measured the internal solid radial displacement profiles in cartilage-subchondral bone samples under unconfined compression [39].

6.2 Ultrasound reflection from the cartilage surface

Reflection coefficient in the frequency domain

A quantitative method for determining the ultrasound reflection coefficient for the cartilage surface was introduced by Chérin *et al.* (1998) [28]. In the following presentation, the linearity of the system (linear acoustics, linear transduction) is assumed and the measurement geometry is a non-contact pulse-echo method in which the sample is immersed in saline.

Let $S_c(z, f)$ be the frequency domain ultrasound signal reflected from the cartilage sample surface back to the ultrasound transducer (z is the distance or depth between the transducer and the cartilage surface and f is the ultrasound frequency). This reflected signal can be presented as follows:

$$S_c(z, f) = E(f) \times G(f) \times A_0(z, f) \times H_s(z, f)^2 \times R_c(f), \tag{6.1}$$

where $E(f)$ is the acoustoelectric transfer function, $G(f)$ is the acquisition system transfer function, $A_0(z,f)$ is the frequency and depth-dependent attenuation function in saline, $H_s(z,f)^2$ is the surface-integrated diffraction function (in the pulse-echo method) and $R_c(f)$ is the ultrasound reflection coefficient for the cartilage surface. The following assumptions are included in the equation (6.1):

1. The sample surface is uniform, *i.e.* the reflection coefficient is constant all over the surface.

2. The sample surface is perpendicular to the incident ultrasound signal and there is no curvature of the surface.

3. The distance between the transducer and each surface point (z) is large enough in comparison with the transducer dimensions. Thus, attenuation and diffraction functions can be separated.

4. The dimensions of the cartilage surface are small as compared to the distance between the transducer and surface (z). Thus, the attenuation term is constant across the surface and $H_s(z,f)^2$ can be defined by integration of the transducer diffraction function over this insonated surface.

In order to calculate the ultrasound reflection coefficient for the cartilage surface ($R_c(f)$ in eq. (6.1)), the attenuation function, the surface-integrated diffraction function and the characteristics of the acquisition system need to be known.

By assuming that the acquisition system is the same as in the cartilage sample measurements, the frequency domain ultrasound signal reflected back from the perfect reflector ($S_r(z,f)$), immersed in saline at the same distance z, can be presented as follows:

$$S_r(z,f) = E(f) \times G(f) \times A_0(z,f) \times H_s(z,f)^2 \times R_r(f), \tag{6.2}$$

where the reflection coefficient of the perfect reflector ($R_r(f)$, *e.g.*, from the water-air interface [127]) is assumed to be independent of the frequency and equal to 1. $R_c(f)$ from equation (6.1) can be presented as follows:

$$R_c(f) = \frac{S_c(z,f)}{E(f) \times G(f) \times A_0(z,f) \times H_s(z,f)^2}. \tag{6.3}$$

By combining equations (6.2) and (6.3) we obtain:

$$R_c(f) = \frac{S_c(z,f)}{S_r(z,f)}. \tag{6.4}$$

With this method, one can eliminate the effects of the attenuation function as well as the surface-integrated diffraction function and the characteristics of the acquisition system. In principle, the ultrasound reflection coefficient for the cartilage surface can be quantified by measuring the ultrasound reflection from both the cartilage surface and from the perfect reflector using any acquisition system and measurement geometry. The frequency spectra, $S_c(z, f)$ and $S_r(z, f)$, are typically determined with the Fast Fourier Transform (FFT) method.

Before conducting FFT, the ultrasound signal is Hamming windowed to include only the reflection from the cartilage surface. Hamming window enhances the contribution of the specular reflection as compared to the scattering occurring beneath the surface. Hamming window operation can be conducted, *e.g.*, with the LabVIEW-software:

$$S_H = S_o \left[0.54 - 0.46 \cos \frac{2\pi i}{n} \right], i = 0, 1, 2, ..., n-1; \tag{6.5}$$

where S_H is the Hamming windowed signal, S_0 is the original unprocessed signal and n is the amount of data (time) points in the window. The Hamming window operation is not needed with a reference signal from the perfect reflector since no scattering occurs in it. After the Hamming window operation, the length of both the cartilage ultrasound signal and the reference signal is expanded with the zero-padding operation. With zero-padding, it is possible to increase the resolution of the frequency domain in FFT.

The energy reflection coefficient for the cartilage surface ($R_c^{dB}(f)$) can be determined as follows:

$$R_c^{dB}(f) = 10 \times \log_{10} \left\langle |R_c(f)|^2 \right\rangle, \tag{6.6}$$

where $\langle ... \rangle$ indicates the spatial average over all scan lines within the 2D ultrasound image. Finally, the integrated reflection coefficient (IRC) is defined as follows:

$$IRC = \frac{1}{\Delta f} \int_{\Delta f} R_c^{dB}(f) df, \tag{6.7}$$

where Δf is the frequency bandwidth.

Reflection coefficient in the time domain

The ultrasound reflection coefficient can also be determined in the time domain. The method makes the same assumptions as in frequency domain analysis. Let A_c be the maximum peak-to-peak amplitude of the time domain ultrasound signal $S_c(z)$ reflected from the cartilage sample surface back to the ultrasound transducer at a distance z (Figure 6.1). Similarly, A_r is the maximum peak-to-peak amplitude for a perfect reflector signal at the same distance z. The ultrasound reflection coefficient for the cartilage surface in the time domain (R_c) can be presented as follows:

$$R_c = \frac{A_c}{A_r} \cdot 100\%. \tag{6.8}$$

The equation (6.8) indicates the relative amount of reflected ultrasound pressure amplitude from the cartilage surface as compared to the perfect reflector.

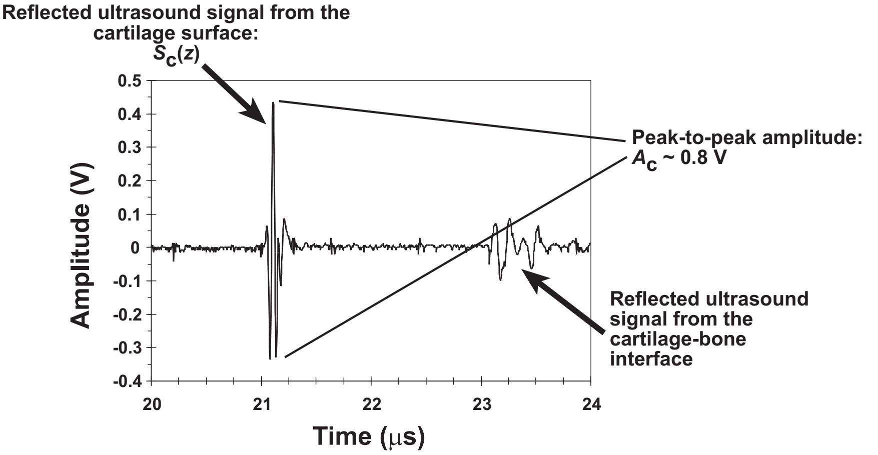

Figure 6.1: Typical ultrasound signal from a healthy bovine articular cartilage measured by the non-contact, pulse-echo technique. Two distinct reflected wavefronts are generated from the cartilage surface and from the cartilage-bone interface. A_c is determined as a peak-to-peak amplitude for the cartilage surface.

6.3 Acoustic properties of articular cartilage

The typical degenerative changes which occur in OA significantly affect the acoustic properties of articular cartilage [28, 52, 94, 97]. In many studies, the acoustic properties have been measured for full thickness cartilage samples. However, as the tissue is inhomogeneous and anisotropic, it would be predicted that acoustic properties would vary as a function of tissue depth as well.

Speed of sound

Speed of sound (measured at 10 MHz) has been reported to be strongly dependent on the cartilage tissue composition, *i.e.* water content, proteoglycan content and collagen content [123]. Furthermore, it has been demonstrated that the orientation of the collagen fibrils significantly affects the sound speed (measured at 100 MHz) [5]. A significant decrease in the sound speed was reported in degenerated cartilage as compared with healthy tissue [52, 94, 123]. The speed of sound in normal cartilage is typically 1600-1770 m/s [94, 123], whereas in degenerated tissue the sound speed is reduced, *i.e.* 1560-1600 m/s [94, 123].

Ultrasound attenuation

In 1990, Agemura *et al.* demonstrated that ultrasound attenuation in cartilage tissue (measured at 100 MHz) is significantly dependent on the integrity of the cross-links in the collagen fibres [5]. In that study, proteoglycan depletion had no effect on the attenuation and speed [5]. However, it was proposed later that attenuation is significantly related to both collagen and proteoglycan contents [96]. Ultrasound attenuation for bovine cartilage tissue has been reported to be 1.8-2.7 dB/mm [96], 2.8-6.5 dB/mm [116] and 92-147 dB/mm [5] at frequency ranges of 5-9 MHz, 10-40 MHz and 100 MHz, respectively. For human articular cartilage, attenuation is 6.2-7.1 dB/mm at the frequency of 30 MHz [52]. Based on these results, it is clear that ultrasound attenuation in cartilage tissue is highly dependent on the frequency used, *i.e.* attenuation increases at higher frequencies.

Ultrasonically determined cartilage thickness

An increase in tissue thickness, measured with ultrasound, has been reported for degenerated cartilage samples compared with intact specimens [28, 78, 114]. Thickness measurements are typically based on the assumption of constant sound speed in tissue and, thus, known variations in site- and depth-dependent composition and structure of articular cartilage may cause uncertainty in the measured thickness values.

Acoustic impedance

Density of articular cartilage tissue is approximately 1050 kg/m^3 [53]. Based on the above results for the speed of sound, *i.e.* 1560-1770 m/s [94, 123], the acoustic impedance of cartilage tissue could be approximated to be $1.64-1.86\times10^6$ kg/m^2/s.

Ultrasound reflection from the cartilage surface and backscattering from the internal tissue

Ultrasound reflection from the cartilage surface (measured at 22-55 MHz) has been proposed to be a sensitive indicator of the superficial cartilage degradation [28, 50, 68, 97, 114, 119, 124], *i.e.* increased surface roughness and degeneration of superficial collagen fibrils taking place during early OA [86]. In contrast, depletion of superficial proteoglycans has no significant effect on the ultrasound reflection coefficient for the surface [70, 103]. The ultrasound reflection coefficient for the cartilage surface in the time domain is approximately 2.6-5.7 % for intact bovine cartilage samples [70, 97, 124]. In the frequency domain, the integrated reflection coefficient (IRC) for intact rat articular cartilage has been reported to be approximately 21-24 dB lower (measured at 50-55 MHz) than the ultrasound reflection from the perfect reflector [28, 29, 103].

Ultrasound backscattering from the internal cartilage matrix has been investigated in rat cartilage tissue [28, 29, 103]. The results demonstrated that backscattering in intact bovine cartilage is approximately 38-52 dB lower (measured at 50-55 MHz) than that determined from the perfect reflector [28, 29, 103]. Furthermore, both the ultrasound reflection coefficient for the cartilage surface as well as backscattering from the internal tissue depend on the maturation stage of the tissue [29, 103].

Based on the existing literature, it can be proposed that porcine [61] or rat [28, 29] internal cartilage tissue scatters ultrasound more effectively than bovine [70, 97] or human [94] tissue. Consequently, it can be hypothesized that quantitative measurement of ultrasound backscattering from the internal human tissue will be quite complicated due to the potentially weak echo signal. However, it can be anticipated that backscattering from the internal tissue will be dependent on the ultrasound frequency and that the backscattering will be probably more intensive at high frequencies.

Ultrasound reflection from the cartilage-bone interface

Quantitative ultrasound analysis of the cartilage-bone interface is challenging as the attenuation, due to both absorption and scattering, in the overlying cartilage tissue may significantly affect the results. It has been qualitatively evaluated that the echogenicity of the cartilage-bone interface increases during OA [34, 72, 73, 114, 119]. Quantitatively, the frequency domain ultrasound reflection and backscattering coefficient for the cartilage-bone interface in intact rat cartilage tissue was reported to be approximately 30-34 dB lower than the ultrasound reflection from the perfect reflector [50]. It is noteworthy that the effect of attenuation in the overlying cartilage tissue was not taken into account in the study [50]. By assuming a constant attenuation coefficient for cartilage, the reflection coefficient in time domain for intact porcine cartilage has been reported to be approximately 15 % [72].

CHAPTER VII

Surface roughness of articular cartilage

7.1 Surface roughness parameters

The surface roughness of materials can be experimentally determined with several techniques. Typically, surface roughness is measured with a stylus profilometer in which the surface profile for a predefined measurement length is determined and, subsequently, a numerical parameter is calculated to indicate the surface roughness. The stylus profilometers set very high requirements for the apparatus and the environmental conditions as even the slightest trembling induces uncertainty into the results. Furthermore, the mechanical profilometer requires direct contact with the examined material, potentially damaging fragile samples such as biological materials.

Optical methods, *e.g.*, laser profilometry, are also widely used for the characterization of material surfaces. The benefit of optical devices, as compared to mechanical profilometers, is that they do not require direct contact with the material surface. In optical devices, the measurement is based on the backscattering of light from the surface, this being detected with highly sensitive detectors.

When defining the statistical parameters for surface roughness it is assumed that the baseline of the measured surface profile is perfectly straight. Then, one can define the average roughness (R_a) and root mean square (RMS) roughness (R_q) as follows:

$$R_a = \frac{1}{L}\int_0^L |y(x)|\,dx, \tag{7.1}$$

$$R_q = \sqrt{\frac{1}{L}\int_0^L y(x)^2 dx}, \tag{7.2}$$

where L is the measurement length on the surface and $y(x)$ is the one-dimensional surface profile. The main difficulty in experimental situation is that the baseline or, more generally, the base surface is not an ideal straight line or plane. This can be eliminated by conducting several measurements from different surface sites to obtain a final roughness value as an average. There are also better alternatives available, *e.g.*, a high-pass filtering may be applied to the measured surface profile by assuming that the variations in the low frequency range reflect only the contours of the surface but not the true surface roughness. Another way to accomplish the elimination of the large surface contour is to fit a smoothing spline to the measured surface profile. After fitting, the smoothing spline is subtracted from the measured profile at every point.

7.2 Ultrasound determination of articular surface roughness

In principle, ultrasound measurements have a great potential for direct determination of cartilage surface roughness. Saïed *et al.* (1997) proposed that defects of 40-50 μm size could be detected on 50 MHz ultrasound 2D (B-scan) images [114]. Moreover, mechanically created macroscopical superficial defects of the cartilage surface (2 to 12 mm in diameter) can be qualitatively detected and semi-quantitatively graded even using a clinical ultrasound (5-12 MHz) instrument [34]. The ultrasonically detected surface fibrillation is believed to originate from the disruption of the subsurface collagen fibrils [28, 50, 97, 114, 124].

In the literature, one method has been described for the determination of cartilage surface roughness using ultrasound [4, 27]. In that method, the amount of backscattered ultrasound energy is measured at different geometrical angles between the ultrasound transducer and cartilage surface using the ultrasound signal ($S_c(t)$, t = time) reflected and backscattered from the cartilage surface to the ultrasound transducer at an incident angle, *i.e.* the angle between the transducer and the surface normal is 0°. The ultrasound signal power (P_0) is defined as follows:

$$P_0 = \int_T [Q_g(0^\circ) S_c(t)]^2 \, dt, \tag{7.3}$$

where T is the length of the time window and $Q_g(0^\circ)$ is the signal amplifying-correction factor at the incident angle. The normalized power at the oblique angle ($P(\theta)$) is defined as follows:

$$P(\theta) = \frac{1}{P_0} \int_T [Q_g(\theta) S_c(\theta, t)]^2 dt, \tag{7.4}$$

where $Q_g(\theta)$ is the amplifying-correction factor at the angle θ and $S_c(\theta, t)$ is the ultrasound signal reflected and backscattered from the cartilage surface to the ultrasound transducer at the angle θ. The signal power (dB) is smaller than zero at every angle $\theta \neq 0$. The rationale for using the amplifying-correction factor is to compensate for the possible change in an electric amplifying at different angles.

According to the acoustic theory, the intensity of backscattered ultrasound from a rough surface can be divided into the coherent and incoherent components [26]. With flat or smooth surfaces, ultrasound backscattering is mainly coherent and specular. In rough surfaces, ultrasound backscattering is mainly incoherent. When measuring the backscattered ultrasound signal for small values of θ, the coherent component dominates the signal intensity. When measuring the backscattered ultrasound signal for larger values of θ, the incoherent component dominates and, therefore, changes in surface roughness can be detected with higher accuracy. As the ultrasound backscattering is measured in the time domain at angles of $25° - 40°$ [27], backscattering values for different angles are averaged. The final mean backscattering value is related to the roughness of the surface. However, this technique provides no direct measure of roughness. Moreover, this method is suitable only under laboratory conditions. At present, no quantitative technique capable of measuring the surface roughness of articular cartilage *in vivo* has been described.

7.3 Values of articular surface roughness

In the literature, there are only a few studies devoted to the quantitative determination of cartilage surface roughness [4, 27, 38, 48]. In the work of Forster *et al.* (1996) a contact stylus profilometer and a non-contact laser profilometer were employed for determining the surface roughness of bovine articular cartilage (n=8 for stylus and n=1 for laser, respectively) [38]. The average roughness (R_a) for healthy tissue was 0.8 μm and 1.6 μm as determined with the laser profilometer and stylus profilometer, respectively [38]. In the work of Hu *et al.* (2001) atomic force microscopy was used to determine the surface roughness of healthy rabbit articular cartilage (n=18) [48]. The average roughness (R_a) was 0.16-0.32 μm [48]. In the work of Chiang *et al.* (1997) laser confocal microscopy was used for the determination of surface roughness of human cartilage tissue in healthy (n=2) and osteoarthritic (n=4) samples [27]. In that study, the RMS roughness (R_q) was determined and values in a range between 5.4-99.2 μm were reported [27].

Chapter VIII

Aims of the present study

Previous studies have indicated that mechano-acoustic methods do provide information on the structure, composition and functional properties of normal and degenerated articular cartilage. The main aims of the present study were:

1. To investigate the sensitivity of a recently developed ultrasound indentation instrument to detect and distinguish different spontaneous degenerative stages in bovine articular cartilage.

2. To investigate the relationship between the mechanical and acoustic properties of cartilage.

3. To investigate the sensitivity of quantitative 2D ultrasound imaging for detection of superficial changes after mechanical, enzymatic or spontaneous degeneration of bovine articular cartilage.

4. To develop a novel methodology for quantification of cartilage surface roughness in ultrasound 2D images.

5. To characterize the ability of quantitative 2D ultrasound imaging for detection of site-dependent variation of the acoustic parameters and collagen content in the bovine knee. The roles of cartilage surface roughness and the collagen content as determinants of ultrasound reflection from the articular surface were also clarified.

6. To investigate the sensitivity of 2D ultrasound imaging to quantitatively detect osteoarthrotic changes occuring in the subchondral bone.

Chapter IX

Materials and Methods

The present thesis consists of five independent studies (I - V). In this section, the materials and methods used in the studies are summarized. An introduction to the study design is presented in Table 9.1.

9.1 Articular cartilage samples and processing protocols

All articular cartilage samples were prepared from bovine knee joints (Figure 9.1). Joints were obtained from a local slaughterhouse (Atria Oyj, Kuopio, Finland). Joints were opened and the samples processed within 5 h postmortem (Studies I-III and V) or stored overnight in the freezer (-20°C) before processing (Study IV). In Study II, part of the samples were extracted from the material of our earlier studies [69, 70].

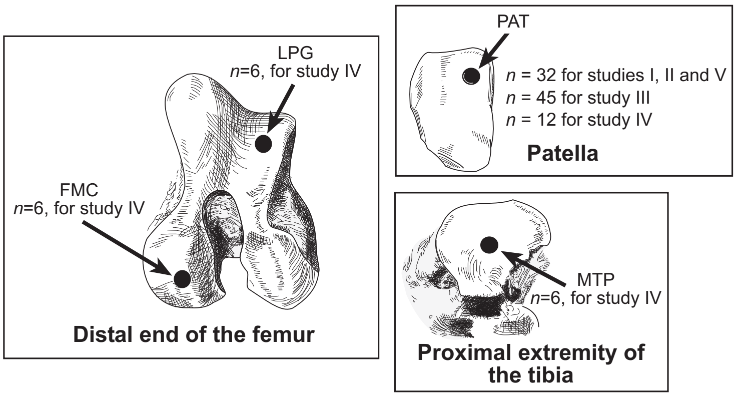
LPG
n=6, for study IV
FMC
n=6, for study IV
Distal end of the femur
PAT
n = 32 for studies I, II and V
n = 45 for study III
n = 12 for study IV
Patella
MTP
n=6, for study IV
Proximal extremity of the tibia

Figure 9.1: Osteochondral samples for all studies were drilled from bovine knee joints. Measurement sites were: medial femoral condyle (FMC), lateral patello-femoral groove (LPG), medial tibial plateau (MTP) and lateral upper quadrant of the patella (PAT).

Table 9.1: Materials and Methods used in the Studies I-V. All articular cartilage samples were prepared from bovine knee joints. Measurement sites are indicated in Figure 9.1. In Study II, part of the samples and results are combined from our earlier studies [69, 70]. All ultrasound and biomechanical measurements were conducted at room temperature (characteristic range 20-23 °C).

Study	Cartilage samples	Methods	Parameters
I	PAT (n=32)	Ultrasound indentation	E_{dyn}, R_i, h
	Normal and spontaneously	Biomechanical reference measurements	E_{DynRef}, E
	degenerated samples	Histological analysis	MS
		Biochemical analysis	H_2O, Uronic
II	PAT (n=32)	Ultrasound indentation	E_{dyn}, R_i, k_{creep}
	Samples from earlier studies:	Biomechanical reference measurements	E_{DynRef}, E
	MTM (n=6), LPG (n=6)	Acoustic reference measurements	c
	MFC (n=6), PAT (n=24)	Histological analysis	MS
III	PAT (n=45)	Ultrasound imaging	R, IRC, URI
	Enzymatically or mechanically		
	degraded samples	Scanning electron microscopy	Qualitative
IV	FMC (n=6), LPG (n=6)	Ultrasound imaging	R, IRC, URI
	MTP (n=6), PAT (n=12)		R_{bone}, IRC_{bone}
		Scanning electron microscopy	Qualitative
		FT-IRIS-analysis	CC
V	PAT (n=32)	Ultrasound imaging	R, IRC, URI
	Normal and spontaneously		R_{bone}, IRC_{bone}
	degenerated samples		
		Scanning electron microscopy	Qualitative
		Acoustic reference measurements	Attenuation
		Biomechanical reference measurements	E_{DynRef}
		Histological analysis	MS

Explanation of the measurement parameters:

E_{dyn}	Dynamic modulus*
R_i	Ultrasound reflection coefficient for the cartilage surface*
h	Cartilage thickness*
k_{creep}	Creep rate*
E_{DynRef}	Reference dynamic modulus**
E	Young's modulus**
MS	Mankin score, as determined histologically using a light microscope
H_2O	Water content, as determined biochemically
Uronic	Uronic acid content, as determined biochemically
c	Speed of sound**
Attenuation	Ultrasound attenuation**
R	Ultrasound reflection coefficient for the cartilage surface in the time domain***
IRC	Ultrasound reflection coefficient for the cartilage surface in the frequency domain***
URI	Ultrasound Roughness Index = cartilage surface roughness***
CC	Amide I absorption (collagen content), as measured with the FT-IRIS technique
R_{bone}	Ultrasound reflection coefficient for the cartilage-bone interface in the time domain***
IRC_{bone}	Ultrasound reflection coefficient for the cartilage-bone interface in the frequency domain***

*As measured with the ultrasound indentation instrument
**As measured with the mechano-acoustic material testing device
***As measured with the 2D ultrasound imaging device.

9.1.1 Enzymatically degraded samples

In Study III, intact bovine knees were collected, opened and specimens from the lateral facets of intact patellar cartilage surfaces were used in the study (Figure 9.1).

Cylindrical osteochondral plugs were taken from the patellae (n=18, diameter=16 mm). Three different enzymes were used for the degradation of the cartilage samples: Collagenase type VII (C 0773, Sigma Chemical Co., St Louis, MO) was utilized for the degradation of the collagen network [117], Chondroitinase ABC (Seikagaku Co., Tokyo, Japan) for the digestion of the proteoglycans [131] and Trypsin (T 0646, Sigma) for proteoglycan digestion with a slight simultaneous effect on the collagen network [44]. The samples were divided into three groups according to the used enzyme: *Collagenase* (n=6), *Chondroitinase ABC* (n=6) and *Trypsin* (n=6). All samples were incubated under physiological conditions (37°C, 5 % CO_2 atmosphere) and immersed in phosphate-buffered saline (PBS) containing antibiotics and the enzyme [124]. A 44 h incubation time was used for Collagenase (30 U/ml) and Chondroitinase ABC (0.1 U/ml) whereas a 60 min incubation time was utilized for Trypsin (1 mg/ml). Quantitative 2D ultrasound images of each sample were collected before and after enzymatic degradations. After the incubations and ultrasound measurements, all samples were stored in a freezer (-20°C). Subsequently, one representative sample from all groups (*Collagenase*, *Chondroitinase ABC* and *Trypsin*) was thawed and processed for the scanning electron microscopy (SEM) of the articular surface.

9.1.2 Mechanically degraded samples

In Study III, intact bovine knees were collected, opened and the lateral facets of intact patellar cartilage surfaces were included in the study (Figure 9.1). Cylindrical osteochondral plugs were taken from the patellae (n=26, diameter=6 mm). Four different emery papers were used (60, 120, 240 and 360 grit) for mechanical degradation of the sample surfaces. Average particle sizes (FEPA standard) of the emery papers used were: 250 μm, 106 μm, 45 μm and 23 μm for 60 grit, 120 grit, 240 grit and 360 grit, respectively. The samples were divided into four groups according to the grade of emery paper used: Paper-60 (n=8), Paper-120 (n=6), Paper-240 (n=6), Paper-360 (n=6). The grinding of sample surfaces was conducted with a custom-made instrument (Figure 9.2). During grinding, the samples were immersed in PBS. The samples were ground under a constant stress (55.5 kPa) with the emery paper glued onto a metallic plate. The grinding protocol was as follows:

1. Constant stress of 55.5 kPa.
2. 10 mm slide against the emery paper.
3. Release of constant stress (55.5 kPa) and 90° rotation of the sample.
4. Constant stress of 55.5 kPa.
5. 10 mm slide against the emery paper.
6. Release of constant stress (55.5 kPa).

Thus, the surface of the cartilage was ground in two perpendicular directions. A quantitative 2D ultrasound image of each sample was collected before and after mechanical grinding. After mechanical degradation and ultrasound measurements, all samples were stored in a freezer (-20°C). Subsequently, one representative sample from each group (*Paper-60*, *Paper-120*, *Paper-240* and *Paper-360*) was thawed and processed for SEM imaging of the articular surface.

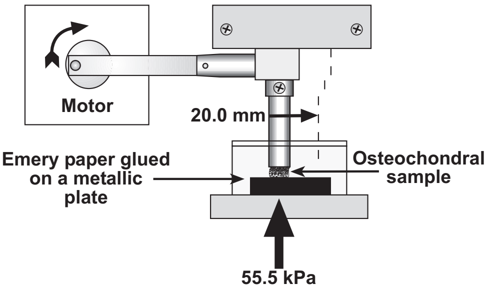

Figure 9.2: Schematic presentation of the cartilage grinding system used for mechanical degradation of the samples.

9.1.3 Spontaneously degenerated samples

In Studies I, II and V, numerous intact bovine knees were collected, opened and the lateral facets of patellar cartilage surfaces (Figure 9.1) were visually graded into four different degenerative grades: *intact*, *slightly discoloured*, *superficial defect* and *deep defect*. Cylindrical osteochondral plugs (n=32, diameter=19 mm) were taken from the specified site of the patella and used for the ultrasound indentation measurements (Studies I and II) or quantitative ultrasound imaging (Study V). Before the measurements, the samples were immersed in PBS containing protease inhibitors and stored in a freezer (-20°C) until measurements.

In the measurements, the samples were thawed and glued to the bottom of a plastic container filled with PBS and protease inhibitors. Initially, mechanical measurements were conducted for the osteochondral sample by using the novel ultrasound indentation instrument (Studies I and II). Second, quantitative 2D ultrasound imaging was conducted at the center of the sample (Study V). After these measurements, the samples were split into two pieces. The first piece of the osteochondral sample was utilized for biomechanical (Studies I,II and V) and biochemical (Study I) reference measurements. The second piece was processed to undergo a histological evaluation (Studies I and V).

9.1.4 Intact samples from bovine knee joint

In Study IV, intact bovine knees were collected, opened and osteochondral blocks (n = 30, diameter=16 mm, Figure 9.1) were processed from the medial femoral condyle (FMC, n = 6), lateral patello-femoral groove (LPG, n = 6), medial tibial plateau

(MTP, $n = 6$) and lateral upper quadrant of patella (PAT, $n = 12$). All samples were imaged with the 2D ultrasound imaging instrument. Subsequently, small slices of osteochondral samples were prepared from the location of ultrasound imaging and processed for the Fourier Transform Infrared spectroscopy (FT-IRIS) analysis. Furthermore, two intact osteochondral samples (10 × 10 × 10 mm) were prepared from PAT and MTP to enable qualitative comparison of surface microtopography with SEM.

9.2 Ultrasound indentation instrument

9.2.1 Experimental measurements

An ultrasound indentation instrument was used in Studies I and II. The instrument [70] consisted of an unfocused, miniature, contact, broadband and an unfocused ultrasound transducer (10.5 MHz, -6 dB bandwidth 5.5-15.5 MHz, diameter=3 mm; Panametrics XMS-310, Panametrics Inc., Waltham, MA, USA) mounted on the tip of a commercial arthroscopic indentation instrument (Artscan 200, Artscan Oy, Helsinki, Finland). This instrument enabled simultaneous measurements of cartilage thickness, deformation and applied stress during indentation test.

Dynamic modulus of the samples was quantified with the ultrasound indentation instrument by generating manually two series of instantaneous compressions on the sample (215 kPa prestress followed by a compressive strain of 4 %). The final dynamic modulus was obtained as a mean of these two measurements. Thickness and deformation of the samples were determined by the time of flight principle using a predefined speed of sound (1627 m/s as measured for the mean ultrasound speed in the bovine cartilage [123]). The dynamic modulus of the samples was calculated using the linear elastic model (see Section 4.3.1) by assuming tissue incompressibility ($\nu = 0.5$).

In addition to dynamic measurements, long-term creep measurements were conducted for four representative samples at different histological stages of degeneration. The protocol for the manual creep measurements consisted of a 1 N (141 kPa) pre-stress for 5 seconds, followed by the test load to induce instantaneously a 4 % strain. The subsequent creep was registered for 20 seconds. The creep rate (k_{creep}), defined as the slope of indentation compliance (C) vs. logarithmic time (C = indentation strain-to-stress ratio, *i.e.* $C = \epsilon/\sigma$), was calculated in order to evaluate the time-dependent behaviour of the tissue.

For the determination of the ultrasound flight time, *i.e.* time between the cartilage surface and the subchondral bone, the Hilbert envelope was calculated for the reflected ultrasound signal and the envelope was Hamming windowed. The ultrasound flight time was tracked in real-time from the point of the maximum value of the Hamming windowed Hilbert-envelope.

After the mechanical indentation measurements, ultrasound reflection from the cartilage surface was determined with the same instrument. In order to keep the transducer at a constant distance from the articular surface, a 3.5 mm long plastic sleeve was attached over the ultrasound transducer. The contact force between the sleeve and the articular surface was continuously monitored and minimized during the measurements. For each sample, the maximum peak-to-peak echo amplitude was measured twice and the average of the amplitudes was calculated. The reflection coefficient was determined according to the equation (6.8).

9.2.2 Finite element modeling

In order to investigate the applicability of the long-term creep measurements conducted with the ultrasound indentation instrument, numerical modeling of cartilage mechanical behaviour was applied in Study II. The manual creep measurements were modeled by using finite element (FE) code (ABAQUS 6.1, Hibbitt, Karlsson & Sorensen Inc., Pawtucket, RI, USA). The axially symmetric transversely isotropic poroelastic model of cartilage consisted of 8-node biquadratic elements (Study II: Figure 4). The material parameters of the model were as follows: Young's modulus (E_1) and Poisson's ratio (ν_{12}) in the transverse plane (*i.e.* the plane of isotropy, parallel to articular surface), out-of-plane (*i.e.* perpendicular to the articular surface) Young's modulus (E_3) and Poisson's ratio (ν_{31}), out-of-plane shear modulus (μ_{13}) and Permeability (k). The initial void ratio, *i.e.* the ratio of fluid to solid content, was 3.5 [89]. The indenter (ultrasound transducer) diameter in the model (3.0 mm) was similar to the transducer diameter used in the ultrasound indentation instrument. Fluid was allowed to flow through the cartilage surface and through the lateral edge, but not through the indenter or fixed cartilage-bone interface, again similar to a realistic measurement situation.

First, the effect of cartilage thickness on the long-term behaviour of tissue was investigated with five different values of cartilage thickness (1, 2, 3, 4 and 5 mm). Material parameters for the model were adopted from the literature (Study II: Table 1). Subsequently, the predefined creep protocol was modeled, and the results of the experimental creep measurements were compared with those of the numerical analyses.

9.3 Quantitative ultrasound imaging

In Studies III and V, the sensitivity of quantitative 2D ultrasound imaging for detecting degenerative changes, such as those typically seen in OA, in cartilage surface or in cartilage-bone interface was investigated. Furthermore, in Study IV, the site-dependent variation for the quantitative ultrasound imaging parameters and the collagen content in the bovine knee was explored.

A Dermascan-C apparatus (Cortex Technology, Hadsund, Denmark) equipped with a 20 MHz focused transducer (spatial sampling interval = 60 μm, beam diameter = 200 μm, focal length = 15 mm, focal zone depth = 3 mm, -6 dB bandwidth = 6-28 MHz) was used for ultrasonic imaging of the samples (Figure 9.3). Raw ultrasound radiofrequency (RF) signals were collected from the Dermascan RF output and digitized at a sampling frequency of 250 MHz with an UltraPAC system (Physical Acoustics Corporation, Princeton, NJ). During imaging, cartilage samples were immersed in PBS and aligned to produce the maximum surface reflection, *i.e.* in order to adjust the surface perpendicular to the transducer axis. Ultrasound RF signals were analyzed with a custom-made LabVIEW 6.1 (National Instruments, Austin, TX) and Matlab 6.0 (The Mathworks Inc., Natick, MA) programs.

Each 2D scan included 160 scan lines corresponding to a distance of 12.1 mm. All ultrasound parameters were calculated from 60 scan lines, at the center of the scan, corresponding to a distance of 4.5 mm. In each scan line, the reflected ultrasound signal from the cartilage surface or from the cartilage-bone interface was windowed (0.6 μs window and 1.0 μs window, respectively) before parameter calculations.

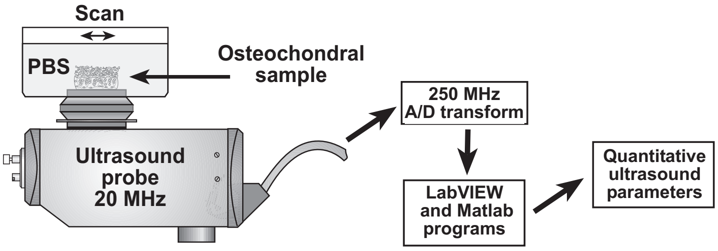

Figure 9.3: Schematic presentation of the ultrasound imaging device used in this study.

9.3.1 Ultrasound reflection parameters

Reference measurements from the perfect reflector

In order to quantitatively calculate the ultrasound reflection coefficients for the cartilage surface, or for the cartilage-bone interface, reference measurements from the perfect reflector at the corresponding distance had to be carried out. Consequently, flight times between the transducer and cartilage surface, or between the transducer and cartilage-bone interface, were quantified line-by-line. For the quantification of the flight times, the Hilbert envelope for the reflected signal was calculated using the fast Hilbert transform and, subsequently, flight time was determined as the location of the maximum value of the envelope. The corresponding distances were calculated by multiplying the flight time by the speed of sound in PBS (1495 m/s at 20°C) or by the speed of sound in cartilage tissue measured specifically for all samples [123].

Subsequently, these distance data were used for the normalization with the reference measurement from the PBS-air interface at the same distance.

Measurements of the reflected amplitude and amplitude spectrum from the PBS-air interface were conducted at 10 different distances covering the whole distance range of the cartilage measurements. The measured reference signals were processed both in the time domain and in the frequency domain. At first, peak-to-peak amplitudes of the reflected signal were calculated for all 10 distances, and an exponential function was fitted to the measured amplitude-distance data. Consequently, the amplitude at any arbitrary distance could be determined from the exponential fit. The amplitude spectra of the reflected signals from the PBS-air interfaces (at 10 distances) were obtained as absolute values of FFT. Furthermore, spline interpolation, included in LabVIEW software, was applied for the determination of amplitude spectra at any arbitrary transducer-cartilage distance. These reference data were used in the calculation of ultrasound reflection parameters for the cartilage surface or for the cartilage-bone interface.

Ultrasound reflection coefficients

Time domain ultrasound reflection coefficients for the cartilage surface (R, %) and for the cartilage-bone interface (R_{bone}, %) were calculated as follows (compare with equation (6.8)):

$$R_x = \frac{1}{m}\sum_{i=1}^{m}\frac{A_i}{A_i^{ref}}\cdot 100\%, \tag{9.1}$$

where m is the number of scan lines ($m = 60$), A_i is the reflected peak-to-peak amplitude from the PBS-cartilage or the cartilage-bone interface in scan line i and A_i^{ref} is the reference peak-to-peak amplitude measured from the PBS-air interface (*i.e.* the perfect reflector) at the same distance as A_i.

The integrated frequency domain reflection coefficients for the cartilage surface (IRC, dB) and for the cartilage-bone interface (IRC_{bone}, dB) were calculated according to equation 6.7, in which Δf is 8-20 MHz and 5-12 MHz for PBS-cartilage interface and cartilage-bone interface, respectively. The lower bandwidth for IRC_{bone} is due to the increased attenuation effect for higher frequencies by the overlying cartilage layer.

In the determination of ultrasound reflection coefficients for the cartilage-bone interface (R_{bone} and IRC_{bone}), sample specific sound reflection at the cartilage surface (R and IRC) and ultrasound attenuation in the overlying cartilage, measured in an earlier study with the same samples [96], were taken into account.

9.3.2 Ultrasound Roughness Index

The microtopography of the cartilage surface was quantified by introducing a novel ultrasound parameter, Ultrasound Roughness Index (URI, μm). URI was determined from the cartilage surface profile using the line-by-line distances (as described above) between the transducer and the PBS-cartilage interface as follows:

$$URI = \sqrt{\frac{1}{m}\sum_{i=1}^{m}(d_i - \langle d \rangle)^2}, \qquad (9.2)$$

where m is the number of scan lines ($m = 60$), d_i is the distance from the transducer to the PBS-cartilage interface in scan line i and $\langle d \rangle$ is the average distance from the transducer to the surface. Before calculation of URI, the natural articular surface contour was eliminated by high-pass-filtering of the surface profile (or fitting a smoothing spline to the measured surface profile), assuming that the true surface roughness is rather in the high frequency range (Study III: Figure 3).

9.4 Reference methods

In order to investigate the sensitivity of the ultrasound indentation instrument as well as quantitative 2D ultrasound imaging for detecting degenerative and site-dependent changes in articular cartilage and subchondral bone, several reference techniques were used. These included mechanical measurements, acoustic measurements, histological analyses, scanning electron microscopy, Fourier transform infrared spectroscopy and biochemical analyses.

9.4.1 Mechano-acoustic measurements

In Studies I, II and V, biomechanical and acoustic reference measurements were conducted with a custom made high-resolution mechano-acoustic material testing device (resolution 0.005 N and 0.1 μm for the force and position, respectively; Figure 9.4). The cartilage plugs (without subchondral bone) were placed between the transducer and a smooth metallic plate in unconfined compression geometry. Mechanical testing was performed using the following stress-relaxation protocol: prestrain = 10 %, strain = 10 %, ramp speed = 2 mm/s, relaxation time = 2400 s. Dynamic modulus and the Young's modulus at equilibrium were determined as a stress per strain ratio instantaneously after a 10 % step and after a 2400 s relaxation time, respectively. Biomechanical reference data were used when investigating the ability of ultrasound indentation and quantitative ultrasound imaging to predict the true mechanical stiffness of cartilage tissue.

An unfocused ultrasound transducer (center frequency = 10.3 MHz, - 3 dB bandwidth = 7.1-14.2 MHz) was used as a compressive plate in the material testing apparatus. The transducer was excited electrically by a 0.5 to 100 MHz pulser-receiver board (PAC-IPR-100, Physical Acoustic Corporation, Princeton, NJ). The ultrasound signal was received by a pulser-receiver board, digitized at 500 MHz by an 8-bit A/D-board (PAC-AD-500, Physical Acoustic Corporation) and stored for later analysis. Acoustic reference measurements included the determination of attenuation and speed of sound [96, 123] in cartilage tissue.

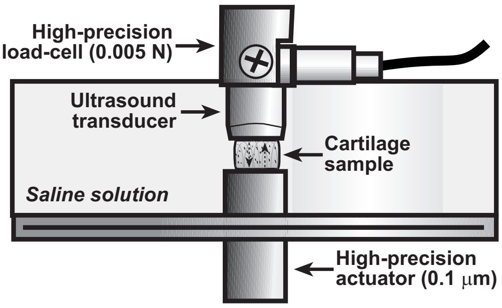
High-precision load-cell (0.005 N)
Ultrasound transducer
Cartilage sample
Saline solution
High-precision actuator (0.1 μm)

Figure 9.4: Schematic presentation of the high-resolution material testing device equipped with the ultrasound transducer. The transducer is in direct contact with the cartilage sample without the subchondral bone. The cartilage sample is compressed to a predefined strain and the force by which the tissue resists the deformation is measured simultaneously as the ultrasound signal is collected. With this configuration, in addition to the mechanical parameters, the speed of sound and attenuation in the tissue can be determined.

9.4.2 Histological and biochemical analyses

In Studies I, II and V, the histological degenerative grade of the samples was obtained with a semi-quantitative histological-histochemical grading system, *i.e.* Mankin scoring system [84]. Using the Mankin score, it is possible to identify different stages of cartilage degeneration by evaluating cartilage structure, cell alterations, safranin-O staining (glycosaminoglycan content) and tidemark integrity (Study I: Table 1). Before evaluation, the samples were randomized and blind-coded. Evaluation was conducted by three investigators and the final Mankin score was obtained as a mean value. In Study V, after histological evaluation, the samples were divided into two groups according to their Mankin score: *intact* (Mankin score = 0, n = 11) and *degenerated* (Mankin score = 1-10, n = 21).

Biochemical analyses, *i.e.* water content and uronic acid content, of the cartilage samples were conducted as described in Study I. The uronic acid content is an indicator of the tissue proteoglycan content [19].

9.4.3 Scanning electron microscopy (SEM)

In Studies III, IV and V, scanning electron microscopy (Philips XL30 ESEM, Fei Co., Eindhoven, Netherlands) was conducted in order to qualitatively visualize the surface structure of normal and degenerated cartilage tissue, and to compare SEM results to those obtained with quantitative ultrasound imaging.

In Study III, a qualitative comparison of normal and mechanically or enzymatically degraded samples (n=8) was conducted with SEM. One sample was selected from each group (*i.e.*, *paper-60*, *paper-120*, *paper-240*, *paper-360*, *collagenase*, *trypsin* and *chondroitinase ABC*). Furthermore, one intact (control) sample without any experimental treatment was selected for SEM evaluation. In Study III, SEM images of articular surface were obtained at a magnification of ×100.

In Study IV, SEM imaging was conducted to visualize the site-specific differences in the structure of the cartilage surface at medial tibial plateau (MTP) and lateral upper quadrant of patella (PAT). In Study IV, SEM images of articular surface were obtained at a magnification of ×1000.

In Study V, SEM imaging of articular surface was conducted for two representative samples. The main aim was to visualize the difference in cartilage surface roughness between a histologically normal sample (Mankin score = 0) and a sample showing histological signs of early degeneration (Mankin score = 2). From the clinical point of view, there is no difference in surface roughness of these samples which can be visually observed, *e.g.*, during arthroscopic examination, but a difference may be determined with SEM or ultrasound imaging.

9.4.4 Fourier transform infrared spectroscopy (FT-IRIS)

In Study IV, the superficial collagen content of the cartilage samples was determined by using the FT-IRIS technique (Perkin Elmer Spotlight 300, Perkin Elmer, Shelton, CO, USA) [25, 105, 111]. After the sample processing (see Study IV for more details) for FT-IRIS measurements, proteoglycans were removed from the samples with hyaluronidase treatment. Subsequently, three sections per sample were transferred onto 2 mm thick ZnSe windows and the FT-IRIS-analyses were conducted as a mean of these three sections. The analysis was limited to the first 100 μm layer of the cartilage surface and the area of the amide I absorption peak (wavenumbers 1710-1610 cm^{-1} with a resolution of 8 cm^{-1}) was used to indicate the collagen content of the sample. In the lateral direction, the mean (±SD) analysis length was 2347 (±443) μm per sample.

9.5 Statistical analyses

The intention of statistical correlation analyses was to reveal the linear relationships between measured variables. In all studies, Spearman's correlation coefficient (r_s) was calculated for the comparison of non-continuous variables (Mankin score), whereas Pearson's correlation coefficient (r) was determined when comparing continuous parameters. The statistical difference between two correlation coefficients was tested by calculating the Fisher Z-transform for both coefficients and, subsequently, evaluating the difference between transformed, normally distributed coefficients.

In Study I, the non-parametric Kruskall-Wallis H and post-hoc tests were used to reveal whether ultrasound indentation measurements could discern between the visually different degenerative grades.

In Study II, the interoperator reproducibility test for the ultrasound indentation instrument was conducted by three investigators. Intraclass correlation coefficients (Rho and 95 % confidence interval) were calculated for the ultrasound indentation parameters (h, E_{dyn} and R). Visually healthy bovine patellar cartilage samples ($n = 8$) were used for the interoperator reproducibility measurements. The reproducibility of the instrument was investigated by calculating the coefficient of variation (CV) and the standardized coefficient of variation (sCV) [17, 42].

In Study III, the non-parametric Wilcoxon signed rank test was applied when evaluating the statistical significance of the difference in ultrasound parameters measured before and after enzymatic or mechanical degradation. The reproducibility (CV and sCV) of the quantitative 2D ultrasound imaging parameters was determined by repeating the same measurement three times on eight control samples with repositioning between successive measurements.

In Study IV, the non-parametric Kruskall-Wallis H test was applied when testing the site-dependent variation of the superficial collagen content and ultrasound imaging parameters of the cartilage surface and of the cartilage-bone interface. The Kruskall-Wallis post-hoc test was used for comparison of the differences in parameters between the individual measurement sites.

In Study V, the non-parametric Mann-Whitney U test was used for the evaluation of statistical differences between the two sample groups.

In all studies, SPSS 8.0-11.5 (SPSS Inc., Chicago, IL, USA) or Matlab 6.0 (The Mathworks Inc., Natick, MA) software was used for statistical analyses.

CHAPTER X

Results

10.1 Ultrasound indentation instrument

10.1.1 Experimental measurements

There was a high linear correlation between the dynamic modulus, measured with the ultrasound indentation instrument, and the reference dynamic modulus, measured with the high-resolution material testing device (Figure 10.1A). Furthermore, the linear correlation within softer (degenerated) samples was also significant (Figure 10.1B). It is notable that some of the visually intact samples exhibited a reduced dynamic stiffness highlighting the insensitivity of visual grading. In study II, in which the results of earlier studies [69, 70] were combined with the results of study I, a strong linear correlation was observed between the dynamic modulus, measured with the ultrasound indentation instrument, and the reference dynamic modulus, measured with the material testing device, in a more heterogenous material (Figure 10.1C). Interestingly, the correlation between the dynamic modulus (ultrasound indentation) and the Young's modulus (reference material testing device) was also significant, though it was lower than that obtained for the correlation between dynamic moduli (Figure 10.1D).

For the determination of dynamic modulus, the agreement between the ultrasound indentation and the reference technique was strongest with the samples of low (<10 MPa) stiffness (Figure 10.2A).

Mankin score, water content, uronic acid content and cartilage stiffness were significantly interrelated with each other. Cartilage dynamic and equilibrium moduli correlated positively ($r \geq 0.717$, $p < 0.05$) with the tissue uronic acid content and negatively ($r \leq -0.586$, $p < 0.05$) with the tissue water content (Study I: Table 3). The cartilage surface reflection coefficient, as measured with the novel instrument, exhibited significant linear correlations with the uronic acid concentration, Mankin score, reference dynamic modulus as well as with the water content (Study I: Figure 4).

Visually different degenerative grades of articular cartilage were distinguished effectively with both mechanical and ultrasound reflection measurements, as conducted with the novel instrument (Figure 10.2B). However, a large variation of the mechanical and acoustic properties was observed within visually intact cartilage samples. Based on the microscopical grading, mean value of Mankin score for the visually intact samples was 0.7 (range=0-3) whereas for the degenerated samples it was 4.3 (range=0-10).

The intraclass correlation coefficients were found to be moderate for all ultrasound indentation parameters (Table 10.1). However, the large confidence intervals diminished the reproducibility of some parameters. CV and sCV values indicated moderate or good reproducibility (Table 10.1).

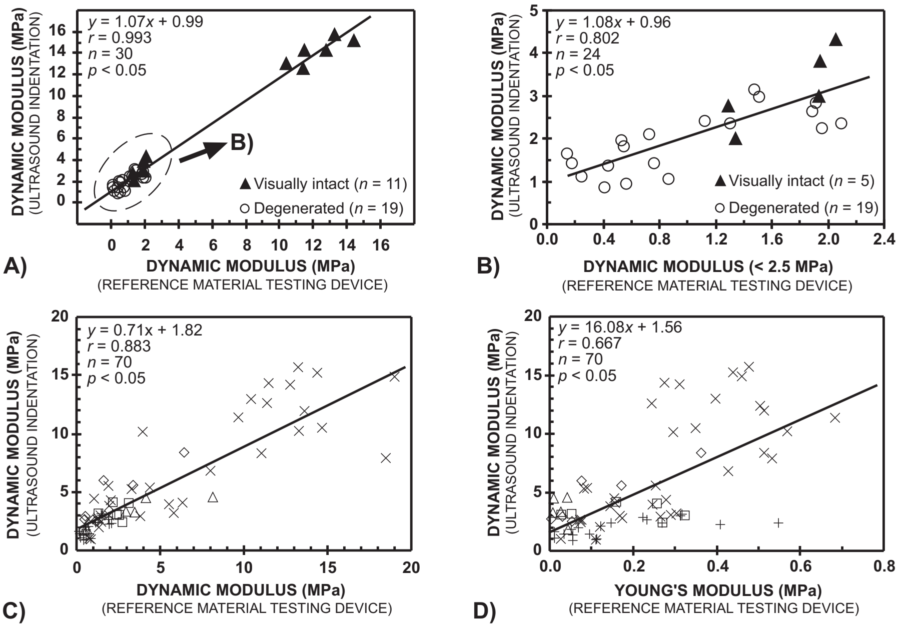

Figure 10.1: A) Linear correlation between the cartilage dynamic modulus, as measured with the ultrasound indentation instrument and the reference dynamic modulus. B) Linear correlation between same parameters among soft (degenerated) samples only. C) Linear correlation between the same parameters in a more heterogenous sample material. D) Linear correlation between the cartilage dynamic modulus, as measured with the ultrasound indentation instrument, and the reference Young's modulus. Symbols used in the figure: visually normal samples (×), visually degenerated samples (+), and samples digested with chondroitinase ABC (□), collagenase (◇) or trypsin (△) [69, 70].

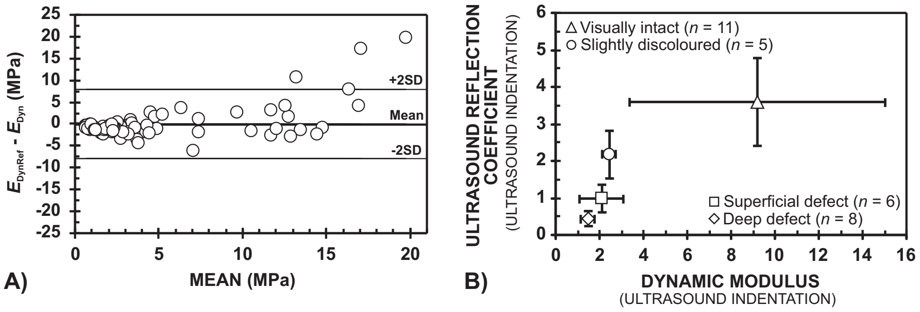

Figure 10.2: A) Bland and Altman plot [18] between the dynamic moduli measured with the reference material testing device (E_{DynRef}) and with the ultrasound indentation instrument (E_{dyn}). B) Mean values (±SD) of the dynamic modulus and ultrasound reflection coefficient, as measured with the ultrasound indentation instrument. The instrument was sensitive of distinguishing between visually different degenerative grades.

Table 10.1: As a measure of interoperator reproducibility of the ultrasound indentation measurements, intraclass correlation coefficient (Rho) for three investigators was calculated for thickness, dynamic modulus and ultrasound reflection coefficient. In addition, the reproducibility was determined in the form of CV and sCV.

Reproducibility	**Thickness** (h)	**Dynamic modulus** (E_{dyn})	**Reflection coefficient** (R)
Intraclass correlation coefficient (Rho)	0.905	0.669	0.786
Coefficient of variation (CV)	5.0 %	17.2 %	5.5 %
Standardized coefficient of variation (sCV)	0.5 %	4.3 %	0.4 %

10.1.2 Finite element modeling

Finite element analyses revealed that the cartilage thickness significantly affected the time-dependent creep, as measured with the ultrasound indentation instrument (Study II: Figure 7). The material parameters used in the numerical model, and experimentally measured creep rates obtained for four samples are presented in Table 10.2. The numerical results agreed well with the experimental findings (Study II: Figure 8).

Significant differences in the material parameters were observed among samples with different degenerative grades (Table 10.2). Young's modulus (E_1 or E_3) and shear modulus (μ_{13}) decreased and permeability (k) increased as the degenerative grade (Mankin score) increased. As seen from Table 10.2, the experimental findings demonstrated also the same trend, *i.e.* E_{dyn} decreased and k_{creep} increased as degeneration progressed.

Table 10.2: Material parameters for the transversely isotropic poroelastic finite element model of articular cartilage and experimentally determined parameters. Numer. and Experim. refer to numerical and experimental results, respectively.

	Numer.	**Numer.**	**Numer.**	**Numer.**	**Numer.**	**Numer.**	**Experim.**	**Experim.**	**Experim.**
	E_1 **(MPa)**	E_3 **(MPa)**	ν_{31}	ν_{12}	μ_{13} **(MPa)**	$k \times 10^{-15}$ **(m^4/Ns)**	E_{dyn} **(MPa)**	k_{creep} **(1/kPa)**	**MS**
Sample 1	16.0	0.44	0.0	0.5	3.20	1.2	15.23	11	0
Sample 2	5.5	0.28	0.0	0.5	1.10	1.8	2.36	18	2
Sample 3	3.1	0.27	0.0	0.5	0.62	5.1	4.32	32	5
Sample 4	0.5	0.03	0.0	0.5	0.10	15.0	1.41	95	10

The explanation of the symbols:

E_1 and ν_{12}	In-plane Young's modulus and Poisson's ratio
E_3 and ν_{31}	Out-of-plane Young's modulus and Poisson's ratio
μ_{13}	Shear modulus
k	Permeability
E_{dyn}	Dynamic modulus measured with the ultrasound indentation instrument
k_{creep}	Creep rate measured with the ultrasound indentation instrument
MS	Histological degenerative grade (Mankin score).

10.2 Relation between cartilage mechanical and acoustic properties

In study II, the relationship between the acoustic and mechanical parameters was investigated in a heterogenous sample material. Significant linear correlations were established between the ultrasound parameters (speed of sound and time domain ultrasound reflection coefficient for the surface) and the cartilage reference mechanical properties (dynamic modulus and Young's modulus) (Figure 10.3). The speed of sound predicted cartilage equilibrium modulus more accurately than the ultrasound surface reflection (correlation coefficients was statistically different, $p < 0.05$). Improved correlation was also observed between the speed of sound and the dynamic modulus ($r = 0.730$), as compared to that between the ultrasound reflection coefficient and the dynamic modulus ($r = 0.562$), although the limit of statistical significance was not reached ($p = 0.09$).

10.3 Quantitative ultrasound imaging

10.3.1 Enzymatically degraded samples

In enzymatically degraded samples, the values of ultrasound reflection coefficients (R and IRC) diminished statistically significantly ($p < 0.05$) after collagenase digestion (Study III: Table 1). Similarly, cartilage surface roughness (URI) increased after collagenase digestion ($p < 0.05$). After chondroitinase ABC or trypsin treatment, no significant changes were seen in the ultrasound imaging parameters (Study III: Table 1). Typical ultrasound image and ultrasonically determined surface profile before and after collagenase digestion are presented in Figure 10.4A. It is notable that,

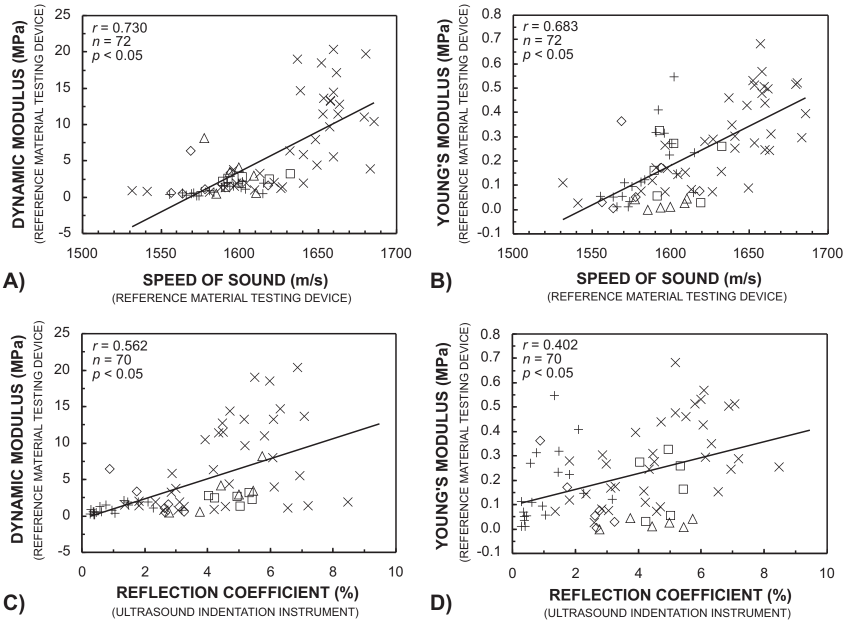

Figure 10.3: Linear correlations between: A) dynamic modulus and speed of sound, B) Young's modulus and speed of sound, C) dynamic modulus and ultrasound reflection coefficient for the surface and D) Young's modulus and ultrasound reflection coefficient for the surface. Dynamic modulus, Young's modulus and speed of sound were measured with the high-resolution mechano-acoustic material testing device. Ultrasound reflection coefficient for the surface was measured with the ultrasound indentation instrument. Significant linear correlations were established between the ultrasound parameters and the mechanical parameters. Symbols used in the figure: visually normal samples (×), visually degenerated samples (+), and samples digested with chondroitinase ABC (□), collagenase (◇) or trypsin (△) [69, 70].

when assessed visually, samples digested with any of the enzymes exhibited normal surface characteristics. However, when the samples were examined using SEM, the degradation of the superficial collagen network could be clearly visualized. SEM images of control (healthy) and enzymatically digested samples are presented in Figure 10.5.

10.3.2 Mechanically degraded samples

In mechanically degraded samples, the values of the ultrasound reflection coefficients (R and IRC) diminished statistically significantly ($p < 0.05$) after grinding with all four emery paper grades (Study III: Table 1). Similarly, surface roughness

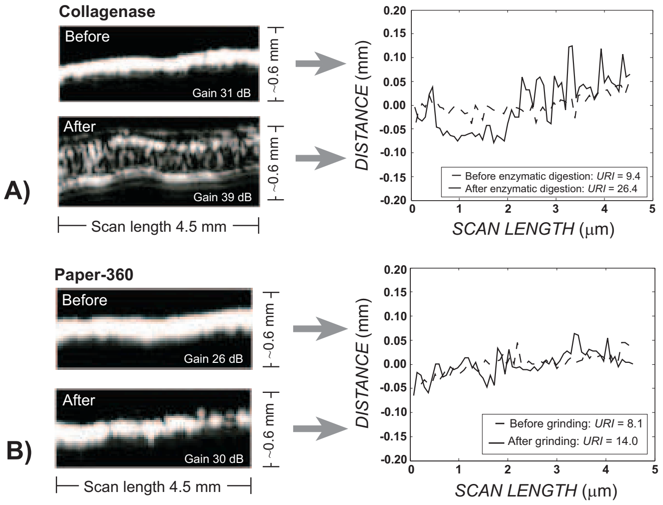

Figure 10.4: Characteristic 2D ultrasound images and ultrasonically determined surface profiles of cartilage samples: A) Before and after collagenase digestion, B) Before and after mechanical degradation with 360 grit (23 μm) emery paper.

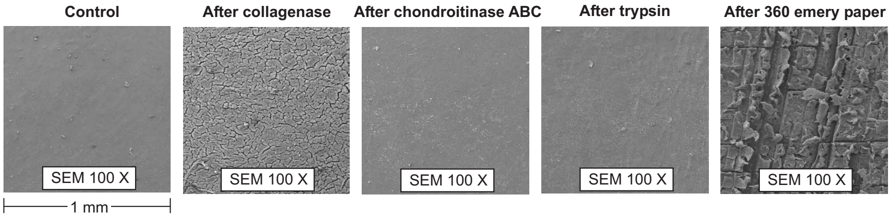
Control
After collagenase
After chondroitinase ABC
After trypsin
After 360 emery paper
SEM 100 X
SEM 100 X
SEM 100 X
SEM 100 X
SEM 100 X
1 mm

Figure 10.5: Scanning electron microscopic (SEM) images of the healthy control sample, enzymatically digested cartilage samples, and sample after mechanical degradation with 360 grit (23 μm) emery paper.

URI increased after mechanical grinding with all emery papers. Typical ultrasound 2D image and ultrasonically determined surface profile before and after mechanical degradation with the smoothest emery paper (360 grit) are presented in Figure 10.4B. It is notable that the samples ground with 360 or 240 grit papers appeared visually normal. However, SEM images of these samples, as seen in Figure 10.5 for 360 grit, revealed a clear degradation of the surface.

10.3.3 Spontaneously degenerated samples

The mean values (± SD) of quantitative ultrasound imaging parameters in *intact* (Mankin score = 0) and histologically *degenerated* (Mankin score = 1-10) sample

Table 10.3: Mean values (±SD) of the quantitative ultrasound imaging parameters and the cartilage reference dynamic modulus in *intact* (Mankin score = 0) and histologically *degenerated* (Mankin score = 1-10) sample groups. Corrected values from the cartilage-bone interface refer to attenuation correction of the overlying cartilage layer.

	Parameter	**Intact (n=11)**	**Degenerated (n=21)**	**Difference (%)**
Cartilage surface:	R (%)	5.3±0.9	2.4±1.6	-54.1*
	IRC (dB)	-26.7±1.6	-34.1±5.5	-27.6*
	URI (μm)	7.4±1.2	24.2±15.5	227.6*
Cartilage-bone interface:	R_{bone} (%)	4.5±1.3	8.9±3.2	98.3*
Uncorrected values	IRC_{bone} (dB)	-25.5±2.5	-19.9±3.9	22.1*
Cartilage-bone interface:	R_{bone} (%)	8.3±2.4	15.0±5.3	80.1*
Corrected values	IRC_{bone} (dB)	-16.9±4.7	-11.0±5.7	34.9*
Biomechanical reference:	E_{dyn} (MPa)	9.5±6.9	1.6±2.4	-83.6*

*Statistically significant difference ($p < 0.05$, Mann-Whitney U test) compared with the intact group.

groups are presented in Table 10.3. A systematic, statistically significant ($p < 0.05$) increase in cartilage surface roughness was observed for degenerated samples as compared to intact specimens (Table 10.3). Furthermore, ultrasound reflection at the cartilage surface underwent a statistically significant ($p < 0.05$) decrease in the degenerated samples.

For ultrasound reflection parameters of the cartilage-bone interface, a statistically significant ($p < 0.05$) increase was observed in degenerated samples compared to intact counterparts (Table 10.3). The attenuation correction affected significantly the measured absolute values of ultrasound reflection from the cartilage-bone interface (Table 10.3).

The same pattern was observed in the reference dynamic modulus, *i.e.* it showed a statistically significant ($p < 0.05$) decrease in degenerated samples (Table 10.3). By using the SEM imaging, increased surface roughness was visualized for the sample with signs of early histological degeneration (Mankin score = 2) compared to the intact (Mankin score = 0) counterpart (Study V: Figure 3).

Significant linear correlations were observed between the ultrasound reflection parameters for the cartilage surface (R, IRC, URI) and the Mankin Score or dynamic modulus ($0.465 < |r| < 0.833$, Study V: Table 2). Generally, R_{bone} and IRC_{bone} did not correlate significantly with the Mankin Score or E_{dyn} ($0.203 < |r| < 0.399$, Study V: Table 2). The attenuation correction of the overlying cartilage had no effect on these correlations ($0.163 < |r| < 0.374$, Study V: Table 2).

Generally, measurements of traditional ultrasound reflection parameters (R and IRC) were reproducible (Table 10.4). The reproducibility of URI, in the form of CV, was lower. However, in the form of sCV, which takes into account the biological variation, better reproducibility was obtained also for URI (Table 10.4).

Table 10.4: Coefficient of variation (CV) and standardized coefficient of variation (sCV) were determined to indicate the reproducibility of the ultrasound imaging parameters. Eight control samples were measured three times with repositioning between measurements.

Reproducibility	R	IRC	URI
Coefficient of variation (CV)	5.2 %	1.3 %	17.0 %
Standardized coefficient of variation (sCV)	2.5 %	1.9 %	5.7 %

10.3.4 Intact samples from bovine knee joint

Articular cartilage thickness, ultrasound reflection coefficients for the surface (R and IRC) as well as surface roughness (URI) showed site-dependent variation within bovine knee ($p < 0.05$, Figure 10.6). Interestingly, cartilage surface roughness, quantified by URI, showed stronger site-dependent variation than the time or frequency domain ultrasound reflection coefficients (Figure 10.6). Qualitatively, SEM images revealed higher surface roughness at MTP than at PAT (Figure 10.7).

The collagen content of the superficial cartilage, as determined by the FT-IRIS technique, was significantly ($p < 0.05$) smaller in FMC than in PAT (Figure 10.8A). The collagen content showed no correlation with the ultrasound surface reflection coefficient (Figure 10.8B), whereas URI exhibited a strong linear correlation with the ultrasound reflection coefficient both in the time ($r = 0.793$, $p < 0.05$, Figure 10.8C) and the frequency domains ($r = 0.813$, $p < 0.05$). However, the linear correlation between URI and collagen content was weak (Figure 10.8D). There was no statistically significant site-dependent variation in the acoustic properties of the cartilage-bone interface (Study IV: Figure 7).

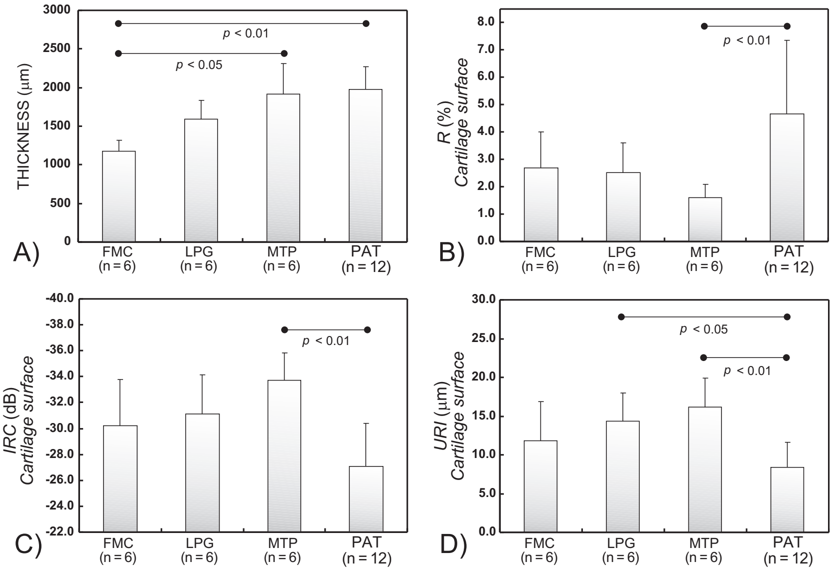

Figure 10.6: Mean values (±SD) of intact cartilage thickness and quantitative ultrasound parameters for the articular surface in different sites within bovine knee joint. A) Cartilage was significantly thinner in the FMC as compared to MTP or PAT. B) A significant difference was observed between MTP and PAT for the ultrasound reflection coefficient in the time domain (R). C) A significant difference was observed between MTP and PAT for the integrated surface reflection coefficient in the frequency domain (IRC). D) Ultrasonically determined surface roughness (URI) was the most sensitive acoustic parameter for detecting differences between different anatomical locations: URI was significantly smaller in PAT, as compared to LPG or MTP.

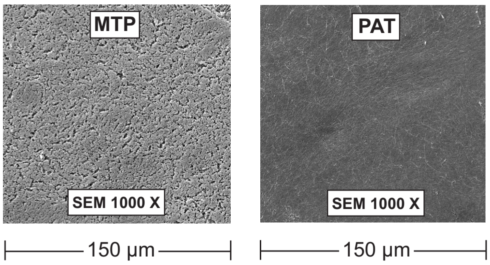

Figure 10.7: Characteristic SEM images of the articular cartilage surface at A) bovine medial tibial plateau (MTP) and B) bovine patella (PAT). In qualitative terms, patellar cartilage surface appeared to be smoother than the tibial surface.

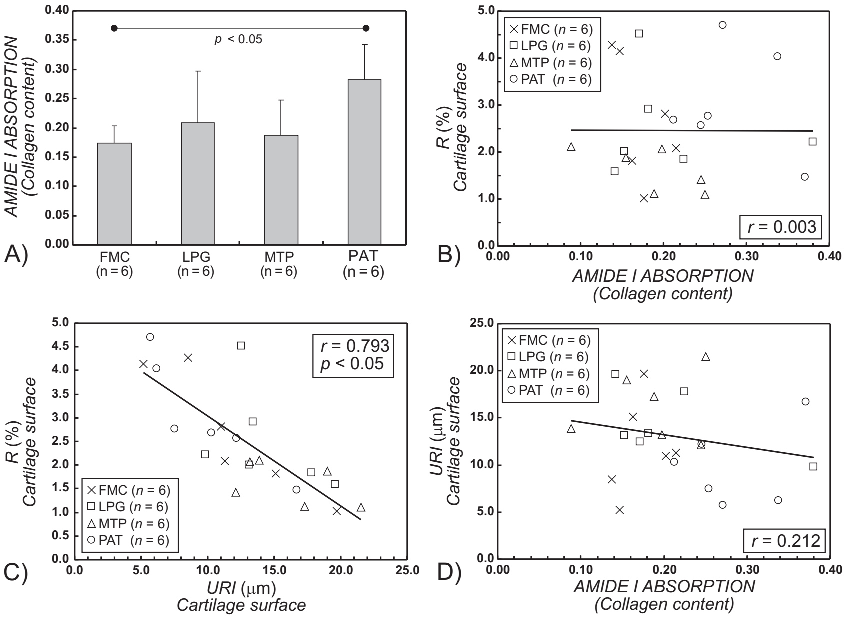

Figure 10.8: A) Mean values (±SD) of superficial collagen content at different anatomical sites within healthy bovine knee joint, as measured by FT-IRIS. B) The linear correlation between the ultrasound reflection coefficient for the cartilage surface in the time domain (R) and the collagen content. C) Cartilage surface roughness, as estimated by URI, was the most sensitive predictor of ultrasound reflection coefficient for the cartilage surface in the time domain (R). D) The linear correlation between URI and cartilage collagen content.

Chapter XI
Discussion

In the present thesis work, the sensitivity of ultrasound indentation technique for detecting and distinguishing spontaneous degenerative stages of bovine articular cartilage was investigated (Study I). The technique was further validated as it is intended for the use during arthroscopic surgery. Furthermore, the ability of combined mechanical and acoustic measurements to improve prediction of cartilage tissue structural and functional integrity was clarified (Study II).

In Study III, the sensitivity of quantitative 2D ultrasound imaging for detecting changes after mechanical or enzymatic degradation was investigated for bovine articular cartilage tissue. Furthermore, a novel parameter, URI, for the quantification of cartilage surface roughness in 2D ultrasound images was introduced (Studies III-V). In Study IV, quantitative ultrasound 2D imaging was utilized to determine ultrasound reflection parameters from the cartilage surface and from the cartilage-bone interface in four anatomical locations of visually healthy bovine knee. In Study V, quantitative 2D ultrasound images were acquired for healthy and spontaneously degenerated bovine articular cartilage samples. The degenerative grade of the samples was determined histologically using the Mankin score method and cartilage compressive modulus was determined as a biomechanical reference.

11.1 Ultrasound indentation instrument

When measuring the stiffness of articular cartilage in indentation geometry, such as is the case in arthroscopic use, the finite and variable tissue thickness affects the indentation response, and introduces uncertainty into the results, especially with thin cartilage [46, 83]. To avoid the uncertainties related to unknown tissue thickness, mechanical indentation and ultrasound were combined in a novel ultrasound indentation instrument [70]. Ultrasound indentation enables a simultaneous measurement of tissue thickness, indentation deformation and stress and, thereby, quantification of tissue intrinsic mechanical properties. In addition to mechanical measurements, ultrasound reflection from the cartilage surface can be determined with the instrument. In that way, the ultrasound reflection coefficient for the cartilage surface can be locally quantified with this novel instrument [70].

In Study I, the dynamic modulus and ultrasound reflection coefficient, both determined with the same instrument, were significantly related to tissue water and uronic acid contents, evidence that the technique does provide information about the cartilage composition. However, these associations are probably complex and follow from the fact that cartilage degeneration is a process in which there are parallel alterations in proteoglycans, collagen network and tissue water content.

Distinct differences between the visually variable degenerative stages could be observed with the measurements of dynamic modulus and ultrasound reflection. The extensive variation of acoustic and mechanical properties within visually intact cartilage samples revealed the insensitivity of visual evaluation for assessing cartilage integrity. This finding was also confirmed by the histological grading (Mankin score) and the biomechanical reference measurements. Some of the visually intact samples exhibited signs of early degeneration, such as depletion of proteoglycans in the superficial tissue, as verified by histological and functional reference measurements. In contrast, the ultrasound indentation instrument distinguished the normal and histologically degenerated cartilage from each other. These results suggest that visual evaluation, conducted routinely during arthroscopy, is inexact and inadequate for judging the functional performance of articular cartilage.

In an earlier study, manual creep measurements were conducted with the ultrasound indentation instrument before and after enzymatic degradation of bovine cartilage samples [70]. It was concluded that the proteoglycan depletion of cartilage could be determined with creep measurements. In Study II, the suitability of creep measurements was further investigated both experimentally and numerically. Poroelastic transversely isotropic FE-model revealed the strong effect of changes in the values of Young's moduli, shear modulus and permeability on the creep behavior. Importantly, this finding was consistent with the experimental measurements revealing a decrease of compressive modulus and an increase of creep rate as the histological degenerative grade (Mankin score) increased. However, successful manual creep measurements with the present instrument require a significant amount of operator training. During arthroscopy, all measurements should be conducted with ease and also quickly and reproducibly. Therefore, it might be necessary to develop the technique further to facilitate long-term creep measurements in the clinic.

In Study II, a strong linear correlation was observed between the dynamic modulus, measured with the ultrasound indentation instrument, and the reference dynamic modulus (measured with the high-resolution material testing device) in a large material ($n = 70$). Furthermore, the interoperator reproducibility, as well as CV and sCV values, indicated moderate or good reproducibility of the ultrasound indentation parameters. As the agreement between the ultrasound indentation and the reference technique was best for the samples with low stiffness, the ultrasound indentation instrument seems to sensitively diagnose early cartilage degeneration.

11.2 Relation between cartilage mechanical and acoustic properties

In Study II, mechano-acoustic techniques were used to characterize the elastic properties of normal and degenerated cartilage in compression. The ability of the acoustic parameters, *i.e.* sound speed and surface reflection, to predict the tissue Young's modulus and dynamic modulus was experimentally studied. It was demonstrated that the sound speed was significantly related to the compressive stiffness as well as the integrity of the tissue. Again, part of these correlations may be secondary, reflecting the complex degenerative process in cartilage tissue with alterations in tissue constituents. In the clinical situation, however, designing a simple and easy-to-use technique for the thickness measurement, necessary for the determination of sound speed, may be difficult and threaten successful diagnostic use. In the literature, one technique, *in situ calibration method*, has actually been introduced for this purpose [121]. However, the need for this kind of complex apparatus possibly will limit its widespread clinical acceptance.

11.3 Quantitative ultrasound imaging

Ultrasound Roughness Index

In Studies III-V, a novel parameter, ultrasound roughness index (URI), was introduced for direct determination of cartilage surface roughness from quantitative ultrasound images. The cartilage surface profile was measured ultrasonically and URI was calculated as the RMS average of deviations from the global surface profile. This method is commonly used in material sciences but has not been earlier adapted to the ultrasonic analysis of cartilage surface topography. The contribution of the global shape (contour) of the cartilage surface was eliminated by high-pass filtering or spline interpolation. In Study III, a significant increase in URI was obtained after mechanical degradation or after collagenase digestion. In Study IV, a significant site-dependent variation was observed for URI within the bovine knee joint. In Study V, URI was significantly higher in histologically degenerated samples with inferior mechanical properties in comparison to intact specimens.

The calculation of URI from the ultrasound 2D image is based on the measurement of ultrasound flight time between the transducer and the PBS-cartilage interface in each scan line. Due to its apparent simplicity, URI might well be able to be incorporated into clinical ultrasound devices, and applied for roughness characterization of different acoustic interfaces within human tissue.

In contrast to traditional reflection parameters (R and IRC), ultrasound flight time does not directly depend on the perpendicularity between the ultrasound transducer and the cartilage surface. This may be a major advantage of URI since achieving perfect perpendicularity is often challenging with naturally curved articular surfaces. Therefore, URI might be easier to use even in arthroscopic ultrasound probes as its calculation requires only the determination of the ultrasound flight time. However, more theoretical and experimental research is still needed: the effects of ultrasound beam diameter, temporal and spatial sampling frequencies and the surface inclination need to be investigated.

In a recent study, ultrasound indentation, ultrasound imaging and MRI results were compared for diagnosing the histological degenerative changes in bovine cartilage tissue [62]. The diagnostic potential of URI was highlighted in that study. The combined sensitivity (0.91) and specificity (1.00) were greatest for URI over other novel diagnostic techniques, including MRI and ultrasound indentation with the novel instrument [62]. The results of that study, along with the present results, suggest that URI, determined with instrumentation that has similar specifications as the one used in the present study, represents a highly sensitive and promising ultrasound parameter for OA diagnostics.

Ultrasound reflection from the cartilage surface

It is generally accepted that ultrasound reflection from the cartilage surface provides an indication of the integrity of the collagen fibril network [28, 68, 97]. In parallel with previous studies, it was found that ultrasound reflection from the tissue surface decreased significantly after collagenase digestion. In contrast to the importance of the collagen fibril network, it has been claimed that proteoglycans play a minor role in ultrasound reflection from the articular surface [97, 103]. Again, this was confirmed in the present thesis work: proteoglycan depletion with chondroitinase ABC induced no significant changes in the ultrasound reflection (or URI) from the surface. In Study V, when investigating ultrasound reflection from the cartilage surface in spontaneously degenerated samples, a statistically significant decrease was observed for R and IRC in degenerated samples compared to intact samples. Furthermore, the results suggest that ultrasound reflection from the cartilage surface also serves as a moderate predictor of cartilage true dynamic stiffness.

Ultrasound reflection from the cartilage-bone interface

Quantitative ultrasound analysis of the cartilage-bone interface is challenging as the attenuation in the overlying cartilage tissue, as well as the reflection at the cartilage surface, may significantly affect the results. In the published literature, ultrasound reflection from the cartilage-bone interface has been quantitatively analyzed without compensating the attenuation effect of the overlying cartilage [50], or by using a constant attenuation coefficient for cartilage [72]. In Study IV, the ultrasound attenuation coefficient in the overlying cartilage was also assumed to be constant.

Consequently, only differences in attenuation due to variable cartilage thickness were taken into account in the calculations of R_{bone} and IRC_{bone}. However, in Study V, the true sample-specific ultrasound attenuation in the overlying cartilage was actually measured, thus confirming its effect on the measured reflection parameters for the cartilage-bone interface. Although the absolute values of R_{bone} and IRC_{bone} increased significantly after attenuation correction, linear correlations between R_{bone} or IRC_{bone} and Mankin score or dynamic modulus were not improved. These results suggest that the changes in cartilage-bone interface, typical to early OA, can be detected without attenuation information. However, in order to determine the absolute values of the reflection coefficients, sound attenuation in the overlying cartilage tissue needs to be known. When aiming at determining R_{bone} and IRC_{bone} arthroscopically *in vivo*, information on cartilage thickness is probably sufficient for acceptable correction of the ultrasound reflection measurements from the cartilage-bone interface.

The exact origin of the ultrasound signal reflecting from the cartilage-bone interface is still under discussion. In earlier studies, it has been hypothesized that this second ultrasound reflection would be generated from the interface between the non-calcified and calcified cartilage, *i.e.* from the tidemark [87, 119]. However, Disler *et al.* (2000) suggested that this ultrasound reflection may be generated at the boundary between the cartilage and subchondral bone [34]. In the present study, no tidemark or calcified cartilage layer could be histologically verified. This may be related to different species (rabbit vs. bovine) or different stages of maturation compared to earlier studies. Consequently, we believe that the second ultrasound reflection in the present samples was generated from the immediate boundary between the cartilage and subchondral bone. Therefore, it reflects the integrity of the subchondral bone. However, in adult human articular cartilage, tidemark and calcified cartilage layer may exist and, in that case, the specular ultrasound reflection may reflect more the integrity of calcified cartilage than that of subchondral bone. This issue needs to be confirmed with human articular cartilage samples.

Site-dependent variation within bovine knee joint

A significant site-dependent variation was shown in quantitative ultrasound imaging parameters for the surface (R, IRC and URI) and for the superficial collagen content. Ultrasound reflection at the cartilage-bone interface (R_{bone} and IRC_{bone}) showed insignificant site-dependent variation. As compared to R and IRC, URI proved to be the most sensitive parameter in detecting differences between the measurement sites. Interestingly, the ultrasound reflection parameters of the surface were not significantly related to superficial collagen content in healthy tissue, whereas there was a high correlation between R and URI. These results suggest that ultrasound reflection from an intact cartilage surface is mainly dependent on the cartilage surface roughness (controlling ultrasound scattering) and that the collagen content (controlling acoustic impedance) has a less significant role. However, it is probable that differences in superficial collagen content are relatively small in different sites within a healthy knee joint. Therefore, a much larger variation in collagen content can be expected for degenerated samples compared to healthy tissue and, in that kind of situation, ultrasound reflection from the tissue surface is possibly related to the superficial collagen content. This issue will require further investigations.

11.4 Diagnostic potential of quantitative ultrasound techniques

Ultrasound indentation instrument

The present results suggest that the ultrasound indentation technique would be capable of determining short-term mechanical properties of cartilage also *in vivo.* The instrument provides direct information on cartilage mechanical function, sensitively impaired in degenerative joint disease, and the *in vivo* measurements can be performed during routine arthroscopy. However, the final judgement of the instrument performance *in vivo* can be done only with human cartilage tissue, measured during real clinical situations. It is also notable that indentation serves as highly pointwise measurement and *in vivo* measurements of certain locations within the knee can be challenging. At this stage, further technical developments of the prototype instrument are needed before it can be used in clinical practice.

Quantitative ultrasound imaging

Based on the present results, quantitative 2D ultrasound imaging enables detection of early experimentally induced or spontaneously developed degenerative changes before degeneration can be visually seen. Furthermore, changes in ultrasound reflection from the cartilage-bone interface can be quantitatively determined with the present ultrasound imaging technique. The major benefit of ultrasound imaging, as compared to more local or point-like measurement techniques, is the possibility to obtain extensive information from large areas of articular surfaces as well as from underneath the cartilage surface. Furthermore, no direct estimation of cartilage surface roughness is possible with the localized techniques.

Quantitative ultrasound imaging is not limited to 2D scans, but is also applicable to 3D measurements. This could be a significant advantage because large areas of the joint can be imaged and reflection or surface roughness values can be obtained pixel-by-pixel in 3D, *e.g.*, during open joint surgery. In principle, the clinical application of these techniques may be achieved by using a high-resolution microarray probe or by one moving (scanning) transducer. This kind of instrumentation sets high demands for the development of an arthroscopic ultrasound imaging device as well as for collection of reference values for ultrasound reflection and surface roughness. At the moment, no prototype of the high-resolution *in vivo* imaging device exists. Therefore, development of the arthroscopic ultrasound imaging instrument will be essential for further clinical investigations.

Chapter XII

Summary and conclusions

In this thesis work, the ultrasound indentation instrument was validated and qualified for further development towards its clinical use. Furthermore, quantitative ultrasound imaging was demonstrated to be a sensitive and specific method for detecting the structural and functional properties of normal and osteoarthrotic articular cartilage tissue.

The main conclusions from the present study are summarized as follows:

1. Dynamic modulus and ultrasound reflection coefficient at the cartilage surface, both measured with the ultrasound indentation instrument, are sensitive for detecting spontaneously developed degenerative histological, compositional and biomechanical changes in bovine cartilage tissue.

2. Mechanical stiffness of cartilage tissue (dynamic modulus or Young's modulus) is more closely related to the sound speed than to the ultrasound reflection from the surface.

3. Quantitative ultrasound imaging parameters for the surface (R, IRC and URI) sensitively detected differences after mechanically or enzymatically (collagenase) degraded bovine cartilage tissue. Furthermore, R, IRC and URI were able to discern histologically normal and degenerated cartilage tissue from each other during spontaneous cartilage degeneration process.

4. A novel parameter for quantification of cartilage surface roughness, URI, was demonstrated to be highly sensitive and specific for osteoarthrotic surface fibrillation of bovine cartilage tissue.

5. R, IRC and URI showed topographical variation across bovine knee joint surfaces, whereas the ultrasound reflection at the cartilage-bone interface (R_{bone} and IRC_{bone}) was not site-dependent. Ultrasound reflection parameters from the intact cartilage surface (R, IRC) were mainly dependent on the cartilage

surface roughness (URI) with the collagen content having a less significant role.

6. Ultrasound reflection at the cartilage-bone interface (R_{bone} and IRC_{bone}) differentiated histologically normal and degenerated tissue from each other during spontaneous cartilage degeneration process. Furthermore, it was quantitatively confirmed that true ultrasound attenuation in the overlying cartilage significantly affects the measured ultrasound reflection values from the cartilage-bone interface.

7. The presented ultrasound indentation and imaging techniques are capable of achieving highly promising results in laboratory measurements. In principle, they can also benefit *in vivo* diagnostics of OA and monitoring of cartilage repair. However, several technical challenges must be solved before they can be succesfully exploited in the clinic.

REFERENCES

[1] Recommendations for the medical management of osteoarthritis of the hip and knee: 2000 update. American College of Rheumatology Subcommittee on Osteoarthritis Guidelines. *Arthritis Rheum*, 43(9):1905–15, 2000.

[2] Adam C, Eckstein F, Milz S, Schulte E, Becker C, and Putz R. The distribution of cartilage thickness in the knee-joints of old-aged individuals-measurement by A-mode ultrasound. *Clin Biomech*, 13(1):1–10, 1998.

[3] Adams J, S. B., Herz PR, Stamper DL, Roberts MJ, Bourquin S, Patel NA, Schneider K, Martin SD, Shortkroff S, Fujimoto JG, and Brezinski ME. High-resolution imaging of progressive articular cartilage degeneration. *J Orthop Res*, 24(4):708–15, 2006.

[4] Adler RS, Dedrick DK, Laing TJ, Chiang EH, Meyer CR, Bland PH, and Rubin JM. Quantitative assessment of cartilage surface roughness in osteoarthritis using high frequency ultrasound. *Ultrasound Med Biol*, 18(1):51–8, 1992.

[5] Agemura DH, O'Brien (Jr) WD, Olerud JE, Chun LE, and Eyre DE. Ultrasonic propagation properties of articular cartilage at 100 MHz. *J Acoust Soc Am*, 87(4):1786–91, 1990.

[6] Amenzade Y. *Theory of Elasticity*. Mir Publishers, Moscow, 1979.

[7] Appleyard RC, Swain MV, Khanna S, and Murrell GA. The accuracy and reliability of a novel handheld dynamic indentation probe for analysing articular cartilage. *Phys Med Biol*, 46(2):541–50, 2001.

[8] Armstrong CG and Mow VC. Variations in the intrinsic mechanical properties of human articular cartilage with age, degeneration, and water content. *J Bone Joint Surg Am*, 64(1):88–94, 1982.

[9] Athanasiou KA, Agarwal A, and Dzida FJ. Comparative study of the intrinsic mechanical properties of the human acetabular and femoral head cartilage. *J Orthop Res*, 12(3):340–9., 1994.

[10] Athanasiou KA, Constantinides G, and Lanctot DR. Articular cartilage evaluator and method for using the same. *United States Patent 5673708*, 1997.

[11] Athanasiou KA, Rosenwasser MP, Buckwalter JA, Malinin TI, and Mow VC. In-

terspecies comparisons of *in situ* intrinsic mechanical properties of distal femoral cartilage. *J Orthop Res*, 9(3):330–40, 1991.

[12] Athanasiou KA, Shah AR, Hernandez RJ, and LeBaron RG. Basic science of articular cartilage repair. *Clin Sports Med*, 20(2):223–47, 2001.

[13] Bader DL and Kempson GE. The short-term compressive properties of adult human articular cartilage. *Biomed Mater Eng*, 4(3):245–56, 1994.

[14] Bailey AJ, Mansell JP, Sims TJ, and Banse X. Biochemical and mechanical properties of subchondral bone in osteoarthritis. *Biorheology*, 41(3-4):349–58, 2004.

[15] Bashir A, Gray ML, Hartke J, and Burstein D. Nondestructive imaging of human cartilage glycosaminoglycan concentration by MRI. *Magn Reson Med*, 41(5):857–65, 1999.

[16] Benedek TG. A history of the understanding of cartilage. *Osteoarthritis Cartilage*, 14(3):203–9, 2006.

[17] Blake GM, Wahner HW, and Fogelman I. Assessment of instrument performance: Precision, installation of new equipment and radiation dose. In *The evaluation of osteoporosis: Dual energy X-ray absorptiometry and ultrasound in clinical practice*, pages 147–157. Martin Dunitz Ltd, London, 2nd edition, 1999.

[18] Bland JM and Altman DG. Statistical methods for assessing agreement between two methods of clinical measurement. *Lancet*, 1(8476):307–10, 1986.

[19] Blumenkrantz N and Asboe-Hansen G. New method for quantitative determination of uronic acids. *Anal Biochem*, 54(2):484–9, 1973.

[20] Brismar BH, Wredmark T, Movin T, Leandersson J, and Svensson O. Observer reliability in the arthroscopic classification of osteoarthritis of the knee. *J Bone Joint Surg Br*, 84(1):42–7, 2002.

[21] Buckwalter J and Mankin H. Articular cartilage, part II: Degeneration and osteoarthritis, repair, regeneration, and transplantation. *J Bone Joint Surg Am*, 79(4):612–32, 1997.

[22] Burstein D and Gray M. New MRI techniques for imaging cartilage. *J Bone Joint Surg Am*, 85-A Suppl 2:70–7, 2003.

[23] Burstein D and Gray ML. Is MRI fulfilling its promise for molecular imaging of cartilage in arthritis? *Osteoarthritis Cartilage*, 2006.

[24] Buschmann MD, Soulhat J, Shirazi-Adl A, Jurvelin JS, and Hunziker EB. Confined compression of articular cartilage: linearity in ramp and sinusoidal tests and the importance of interdigitation and incomplete confinement. *J Biomech*, 31(2):171–8., 1998.

[25] Camacho NP, West P, Torzilli PA, and Mendelsohn R. FTIR microscopic imaging of collagen and proteoglycan in bovine cartilage. *Biopolymers*, 62(1):1–8, 2001.

[26] Chiang EH, Adler RS, Meyer CR, Rubin JM, Dedrick DK, and Laing TJ. Quantitative assessment of surface roughness using backscattered ultrasound: the effects of finite surface curvature. *Ultrasound Med Biol*, 20(2):123–35, 1994.

[27] Chiang EH, Laing TJ, Meyer CR, Boes JL, Rubin JM, and Adler RS. Ultrasonic characterization of *in vitro* osteoarthritic articular cartilage with validation by confocal microscopy. *Ultrasound Med Biol*, 23(2):205–13, 1997.

[28] Chérin E, Saïed A, Laugier P, Netter P, and Berger G. Evaluation of acoustical parameter sensitivity to age-related and osteoarthritic changes in articular cartilage using $50-$ MHz ultrasound. *Ultrasound Med Biol*, 24(3):341–54, 1998.

[29] Chérin E, Saïed A, Pellaumail B, Loeuille D, Laugier P, Gillet P, Netter P, and Berger G. Assessment of rat articular cartilage maturation using 50-MHz quantitative ultrasonography. *Osteoarthritis Cartilage*, 9(2):178–86, 2001.

[30] Dashefsky JH. Arthroscopic measurement of chondromalacia of patella cartilage using a microminiature pressure transducer. *Arthroscopy*, 3(2):80–5, 1987.

[31] Day JS, Van Der Linden JC, Bank RA, Ding M, Hvid I, Sumner DR, and Weinans H. Adaptation of subchondral bone in osteoarthritis. *Biorheology*, 41(3-4):359–68, 2004.

[32] Dervin GF, Stiell IG, Rody K, and Grabowski J. Effect of arthroscopic debridement for osteoarthritis of the knee on health-related quality of life. *J Bone Joint Surg Am*, 85-A(1):10–9, 2003.

[33] DiSilvestro MR and Suh JK. A cross-validation of the biphasic poroviscoelastic model of articular cartilage in unconfined compression, indentation, and confined compression. *J Biomech*, 34(4):519–25, 2001.

[34] Disler DG, Raymond E, May DA, Wayne JS, and McCauley TR. Articular cartilage defects: *In vitro* evaluation of accuracy and interobserver reliability for detection and grading with US. *Radiology*, 215(3):846–51, 2000.

[35] Drexler W, Stamper D, Jesser C, Li X, Pitris C, Saunders K, Martin S, Lodge MB, Fujimoto JG, and Brezinski ME. Correlation of collagen organization with polarization sensitive imaging of *in vitro* cartilage: implications for osteoarthritis. *J Rheumatol*, 28(6):1311–8, 2001.

[36] Duck FA, Baker AC, and Starritt HC, editors. *Ultrasound in medicine*. Medical Science Series. Institute of Physics Publishing, London, 1998.

[37] Elders MJ. The increasing impact of arthritis on public health. *J Rheumatol Suppl*, 60:6–8, 2000.

[38] Forster H and Fisher J. The influence of loading time and lubricant on the friction of articular cartilage. *Proc Inst Mech Eng [H]*, 210(2):109–19, 1996.

[39] Fortin M, Buschmann MD, Bertrand MJ, Foster FS, and Ophir J. Dynamic measurement of internal solid displacement in articular cartilage using ultrasound backscatter. *J Biomech*, 36(3):443–7, 2003.

[40] Fortin M, Soulhat J, Shirazi-Adl A, Hunziker EB, and Buschmann MD. Unconfined compression of articular cartilage: nonlinear behavior and comparison with a fibril-reinforced biphasic model. *J Biomech Eng*, 122(2):189–95., 2000.

[41] Garon M, Legare A, Guardo R, Savard P, and Buschmann MD. Streaming potentials maps are spatially resolved indicators of amplitude, frequency and ionic strength dependant responses of articular cartilage to load. *J Biomech*, 35(2):207–16, 2002.

[42] Glüer CC, Blake G, Lu Y, Blunt BA, Jergas M, and Genant HK. Accurate assessment of precision errors: how to measure the reproducibility of bone densitometry techniques. *Osteoporos Int*, 5(4):262–70, 1995.

[43] Guilak F, Ratcliffe A, Lane N, Rosenwasser MP, and Mow VC. Mechanical and biochemical changes in the superficial zone of articular cartilage in canine experimental

osteoarthritis. *J Orthop Res*, 12(4):474–84., 1994.

[44] Harris (Jr) ED, Parker HG, Radin EL, and Krane SM. Effects of proteolytic enzymes on structural and mechanical properties of cartilage. *Arthritis Rheum*, 15(5):497–503, 1972.

[45] Hattori K, Mori K, Habata T, Takakura Y, and Ikeuchi K. Measurement of the mechanical condition of articular cartilage with an ultrasonic probe: quantitative evaluation using wavelet transformation. *Clin Biomech (Bristol, Avon)*, 18(6):553–7, 2003.

[46] Hayes WC, Keer LM, Herrmann G, and Mockros LF. A mathematical analysis for indentation tests of articular cartilage. *J Biomech*, 5(5):541–51, 1972.

[47] Herrmann JM, Pitris C, Bouma BE, Boppart SA, Jesser CA, Stamper DL, Fujimoto JG, and Brezinski ME. High resolution imaging of normal and osteoarthritic cartilage with optical coherence tomography. *J Rheumatol*, 26(3):627–35, 1999.

[48] Hu K, Radhakrishnan P, Patel RV, and Mao JJ. Regional structural and viscoelastic properties of fibrocartilage upon dynamic nanoindentation of the articular condyle. *J Struct Biol*, 136(1):46–52, 2001.

[49] Hunziker EB. Articular cartilage repair: basic science and clinical progress. a review of the current status and prospects. *Osteoarthritis Cartilage*, 10(6):432–63, 2002.

[50] Jaffre B, Watrin A, Loeuille D, Gillet P, Netter P, Laugier P, and Saied A. Effects of antiinflammatory drugs on arthritic cartilage: a high-frequency quantitative ultrasound study in rats. *Arthritis Rheum*, 48(6):1594–601, 2003.

[51] James CB and Uhl TL. A review of articular cartilage pathology and the use of glucosamine sulfate. *J Athl Train*, 36(4):413–419, 2001.

[52] Joiner GA, Bogoch ER, Pritzker KP, Buschmann MD, Chevrier A, and Foster FS. High frequency acoustic parameters of human and bovine articular cartilage following experimentally-induced matrix degradation. *Ultrason Imaging*, 23(2):106–16, 2001.

[53] Joseph D, Gu WY, Mao XG, Lai WM, and Mow VC. True density of normal and enzymatically treated bovine articular cartilage. *Trans Orthop Res Soc*, 24:642, 1999.

[54] Jurvelin JS, Arokoski JP, Hunziker EB, and Helminen HJ. Topographical variation of the elastic properties of articular cartilage in the canine knee. *J Biomech*, 33(6):669–75, 2000.

[55] Jurvelin JS, Buschmann MD, and Hunziker EB. Optical and mechanical determination of poisson's ratio of adult bovine humeral articular cartilage. *J Biomech*, 30(3):235–41, 1997.

[56] Jurvelin JS, Buschmann MD, and Hunziker EB. Mechanical anisotropy of the human knee articular cartilage in compression. *Proc Inst Mech Eng [H]*, 217(3):215–9, 2003.

[57] Karsdal MA, Tanko LB, Riis BJ, Sondergard BC, Henriksen K, Altman RD, Qvist P, and Christiansen C. Calcitonin is involved in cartilage homeostasis: is calcitonin a treatment for OA? *Osteoarthritis Cartilage*, 14(7):617–24, 2006.

[58] Kawchuk GN and Elliott PD. Validation of displacement measurements obtained from ultrasonic images during indentation testing. *Ultrasound Med Biol*, 24(1):105–

11, 1998.

[59] Kempson GE, Spivey CJ, Swanson SA, and Freeman MA. Patterns of cartilage stiffness on normal and degenerate human femoral heads. *J Biomech*, 4(6):597–609, 1971.

[60] Khalsa PS and Eisenberg SR. Compressive behavior of articular cartilage is not completely explained by proteoglycan osmotic pressure. *J Biomech*, 30(6):589–94., 1997.

[61] Kim HK, Babyn PS, Harasiewicz KA, Gahunia HK, Pritzker KPH, and Foster FS. Imaging of immature articular cartilage using ultrasound backscatter microscopy at 50 MHz. *J Orthop Res*, 13(6):963–70, 1995.

[62] Kiviranta P, Töyräs J, Nieminen MT, Laasanen MS, Saarakkala S, Nieminen HJ, Nissi MJ, and Jurvelin JS. Comparison of novel clinically applicable methodology for sensitive diagnostics of cartilage degeneration. *European Cells and Materials*, Submitted, 2007.

[63] Korhonen RK, Laasanen MS, Toyras J, Rieppo J, Hirvonen J, Helminen HJ, and Jurvelin JS. Comparison of the equilibrium response of articular cartilage in unconfined compression, confined compression and indentation. *J Biomech*, 35(7):903–9, 2002.

[64] Korhonen RK, Laasanen MS, Töyräs J, Lappalainen R, Helminen HJ, and Jurvelin JS. Fibril reinforced poroelastic model predicts specifically mechanical behavior of normal, proteoglycan depleted and collagen degraded articular cartilage. *J Biomech*, 36(9):1373–9, 2003.

[65] Korhonen RK, Saarakkala S, Töyräs J, Laasanen MS, Kiviranta I, and Jurvelin JS. Experimental and numerical validation for the novel configuration of an arthroscopic indentation instrument. *Phys Med Biol*, 48(11):1565–76, 2003.

[66] Korhonen RK, Wong M, Arokoski J, Lindgren R, Helminen HJ, Hunziker EB, and Jurvelin JS. Importance of the superficial tissue layer for the indentation stiffness of articular cartilage. *Med Eng Phys*, 24(2):99–108, 2002.

[67] Kurkijärvi JE, Nissi MJ, Kiviranta I, Jurvelin JS, and Nieminen MT. Delayed gadolinium-enhanced MRI of cartilage (dGEMRIC) and T2 characteristics of human knee articular cartilage: topographical variation and relationships to mechanical properties. *Magn Reson Med*, 52(1):41–6, 2004.

[68] Kuroki H, Nakagawa Y, Mori K, Kobayashi M, Yasura K, Okamoto Y, Mizuno Y, Ando K, Ikeuchi K, and Nakamura T. Maturation-dependent change and regional variations in acoustic stiffness of rabbit articular cartilage: an examination of the superficial collagen-rich zone of cartilage. *Osteoarthritis Cartilage*, 14(8):784–92, 2006.

[69] Laasanen MS, Saarakkala S, Töyräs J, Hirvonen J, Rieppo J, Korhonen RK, and Jurvelin JS. Ultrasound indentation of bovine knee articular cartilage in situ. *J Biomech*, 36(9):1259–67, 2003.

[70] Laasanen MS, Töyräs J, Hirvonen J, Saarakkala S, Korhonen RK, Nieminen MT, Kiviranta I, and Jurvelin JS. Novel mechano-acoustic technique and instrument for diagnosis of cartilage degeneration. *Physiol Meas*, 23:491–503, 2002.

[71] Laasanen MS, Töyräs J, Korhonen RK, Rieppo J, Saarakkala S, Nieminen MT, Hirvonen J, and Jurvelin JS. Biomechanical properties of knee articular cartilage. *Biorheology*, 40(1-3):133–40, 2003.

[72] Laasanen MS, Töyräs J, Vasara A, Saarakkala S, Hyttinen MM, Kiviranta I, and Jurvelin JS. Quantitative ultrasound imaging of spontaneous repair of porcine cartilage. *Osteoarthritis Cartilage*, 14(3):258–63, 2006.

[73] Laasanen MS, Töyräs J, Vasara AI, Hyttinen MM, Saarakkala S, Hirvonen J, Jurvelin JS, and Kiviranta I. Mechano-acoustic diagnosis of cartilage degeneration and repair. *J Bone Joint Surg Am*, 85-A Suppl 2:78–84, 2003.

[74] Lai WM, Hou JS, and Mow VC. A triphasic theory for the swelling and deformation behaviors of articular cartilage. *J Biomech Eng*, 113(3):245–58, 1991.

[75] Lammentausta E, Kiviranta P, Nissi MJ, Laasanen MS, Kiviranta I, Nieminen MT, and Jurvelin JS. T2 relaxation time and delayed gadolinium-enhanced MRI of cartilage (dGEMRIC) of human patellar cartilage at 1.5 T and 9.4 T: Relationships with tissue mechanical properties. *J Orthop Res*, 24(3):366–74, 2006.

[76] Lammi MJ, Qu CJ, Laasanen MS, Saarakkala S, Rieppo J, Jurvelin JS, and Toyras J. Undersulfated chondroitin sulfate does not increase in osteoarthritic cartilage. *J Rheumatol*, 31(12):2449–53, 2004.

[77] Lee RC, Frank EH, Grodzinsky AJ, and Roylance DK. Oscillatory compressional behavior of articular cartilage and its associated electromechanical properties. *J Biomech Eng*, 103(4):280–92., 1981.

[78] Lefebvre F, Graillat N, Chérin E, Berger G, and Saïed A. Automatic three-dimensional reconstruction and characterization of articular cartilage from high-resolution ultrasound acquisitions. *Ultrasound Med Biol*, 24(9):1369–81, 1998.

[79] Legare A, Garon M, Guardo R, Savard P, Poole AR, and Buschmann MD. Detection and analysis of cartilage degeneration by spatially resolved streaming potentials. *J Orthop Res*, 20(4):819–26, 2002.

[80] Li X, Martin S, Pitris C, Ghanta R, Stamper DL, Harman M, Fujimoto JG, and Brezinski ME. High-resolution optical coherence tomographic imaging of osteoarthritic cartilage during open knee surgery. *Arthritis Res Ther*, 7(2):R318–23, 2005.

[81] Lyyra T, Jurvelin J, Pitkänen P, Väätäinen U, and Kiviranta I. Indentation instrument for the measurement of cartilage stiffness under arthroscopic control. *Med Eng Phys*, 17(5):395–9, 1995.

[82] Mak AF. The apparent viscoelastic behavior of articular cartilage–the contributions from the intrinsic matrix viscoelasticity and interstitial fluid flows. *J Biomech Eng*, 108(2):123–30, 1986.

[83] Mak AF, Lai WM, and Mow VC. Biphasic indentation of articular cartilage. I. Theoretical analysis. *J Biomech*, 20(7):703–14, 1987.

[84] Mankin HJ, Dorfman H, Lippiello L, and Zarins A. Biochemical and metabolic abnormalities in articular cartilage from osteo-arthritic human hips. II. Correlation of morphology with biochemical and metabolic data. *J Bone Joint Surg Am*, 53(3):523–37, 1971.

[85] Mankin HJ and Thrasher AZ. Water content and binding in normal and osteoarthritic human cartilage. *J Bone Joint Surg Am*, 57(1):76–80, 1975.

[86] Minns RJ, Steven FS, and Hardinge K. Osteoarthrotic articular cartilage lesions of the femoral head observed in the scanning electron microscope. *J Pathol*, 122(2):63–70, 1977.

[87] Modest VE, Murphy MC, and Mann RW. Optical verification of a technique for *in situ* ultrasonic measurement of articular cartilage thickness. *J Biomech*, 22(2):171–6, 1989.

[88] Moseley JB, O'Malley K, Petersen NJ, Menke TJ, Brody BA, Kuykendall DH, Hollingsworth JC, Ashton CM, and Wray NP. A controlled trial of arthroscopic surgery for osteoarthritis of the knee. *N Engl J Med*, 347(2):81–8, 2002.

[89] Mow VC, Fithian DC, and Kelly MA. Fundamentals of articular cartilage and meniscus biomechanics. In Ewing JW, editor, *Articular cartilage and knee joint function: basic science and arthroscopy*, pages 1–18. Raven Press Ltd., New York, 1990.

[90] Mow VC and Guo XE. Mechano-electrochemical properties of articular cartilage: Their inhomogeneities and anisotropies. *Annu Rev Biomed Eng*, 4:175–209, 2002.

[91] Mow VC, Kuei SC, Lai WM, and Armstrong CG. Biphasic creep and stress relaxation of articular cartilage in compression: Theory and experiments. *J Biomech Eng*, 102(1):73–84, 1980.

[92] Mow VC, Ratcliffe A, and Poole AR. Cartilage and diarthrodial joints as paradigms for hierarchical materials and structures. *Biomaterials*, 13(2):67–97, 1992.

[93] Myers E and Mow VC. Biomechanics of cartilage and its response to biomechanical stimuli. *Cartilage, Structure, Function, and Biochemistry*, 1:313–341, 1983.

[94] Myers SL, Dines K, Brandt DA, Brandt KD, and Albrecht ME. Experimental assessment by high frequency ultrasound of articular cartilage thickness and osteoarthritic changes. *J Rheumatol*, 22(1):109–16, 1995.

[95] Niederauer MQ, Cristante S, Niederauer GM, Wilkes RP, Singh SM, Messina DF, Walter MA, Boyan BD, DeLee JC, and Niederauer G. A novel instrument for quantitatively measuring the stiffness of articular cartilage. *Trans Orthop Res Soc*, 23:905, 1998.

[96] Nieminen HJ, Saarakkala S, Laasanen MS, Hirvonen J, Jurvelin JS, and Töyräs J. Ultrasound attenuation in normal and spontaneously degenerated articular cartilage. *Ultrasound Med Biol*, 30(4):493–500, 2004.

[97] Nieminen HJ, Töyräs J, Rieppo J, Nieminen MT, Hirvonen J, Korhonen R, and Jurvelin JS. Real-time ultrasound analysis of articular cartilage degradation in vitro. *Ultrasound Med Biol*, 28(4):519–25, 2002.

[98] Nieminen MT, Rieppo J, Silvennoinen J, Töyräs J, Hakumäki JM, Hyttinen MM, Helminen HJ, and Jurvelin JS. Spatial assessment of articular cartilage proteoglycans with Gd-DTPA-enhanced T1 imaging. *Magn Reson Med*, 48(4):640–8, 2002.

[99] Nieminen MT, Rieppo J, Töyräs J, Hakumäki JM, Silvennoinen J, Hyttinen MM, Helminen HJ, and Jurvelin JS. T2 relaxation reveals spatial collagen architecture in articular cartilage: a comparative quantitative MRI and polarized light microscopic

study. *Magn Reson Med*, 46(3):487–93, 2001.

[100] Nieminen MT, Töyräs J, Rieppo J, Hakumäki JM, Silvennoinen J, Helminen HJ, and Jurvelin JS. Quantitative MR microscopy of enzymatically degraded articular cartilage. *Magn Reson Med*, 43(5):676–81, 2000.

[101] Pagnano M and Westrich G. Successful nonoperative management of chronic osteoarthritis pain of the knee: safety and efficacy of retreatment with intra-articular hyaluronans. *Osteoarthritis Cartilage*, 13(9):751–61, 2005.

[102] Pan Y, Li Z, Xie T, and Chu CR. Hand-held arthroscopic optical coherence tomography for *in vivo* high-resolution imaging of articular cartilage. *J Biomed Opt*, 8(4):648–54, 2003.

[103] Pellaumail B, Watrin A, Loeuille D, Netter P, Berger G, Laugier P, and Saïed A. Effect of articular cartilage proteoglycan depletion on high frequency ultrasound backscatter. *Osteoarthritis Cartilage*, 10(7):535–41, 2002.

[104] Poole AR, Kojima T, Yasuda T, Mwale F, Kobayashi M, and Laverty S. Composition and structure of articular cartilage: a template for tissue repair. *Clin Orthop Relat Res*, (391 Suppl):S26–33, 2001.

[105] Potter K, Kidder LH, Levin IW, Lewis EN, and Spencer RG. Imaging of collagen and proteoglycan in cartilage sections using Fourier transform infrared spectral imaging. *Arthritis Rheum*, 44(4):846–55, 2001.

[106] Qin L, Zheng Y, Leung C, Mak A, Choy W, and Chan K. Ultrasound detection of trypsin-treated articular cartilage: its association with cartilaginous proteoglycans assessed by histological and biochemical methods. *J Bone Miner Metab*, 20(5):281–7, 2002.

[107] Qu CJ, Karjalainen HM, Helminen HJ, and Lammi MJ. The lack of effect of glucosamine sulphate on aggrecan mRNA expression and (35)S-sulphate incorporation in bovine primary chondrocytes. *Biochim Biophys Acta*, 1762(4):453–9, 2006.

[108] Quenneville E, Binette JS, Garon M, Legare A, Meunier M, and Buschmann MD. Fabrication and characterization of nonplanar microelectrode array circuits for use in arthroscopic diagnosis of cartilage diseases. *IEEE Trans Biomed Eng*, 51(12):2164–73, 2004.

[109] Radin EL, Paul IL, and Lowy M. A comparison of the dynamic force transmitting properties of subchondral bone and articular cartilage. *J Bone Joint Surg Am*, 52(3):444–56., 1970.

[110] Radin EL and Rose RM. Role of subchondral bone in the initiation and progression of cartilage damage. *Clin Orthop Relat Res*, (213):34–40, 1986.

[111] Rieppo J, Hyttinen MM, Jurvelin JS, and Helminen HJ. Reference sample method reduces the error caused by variable cryosection thickness in fourier transform infrared imaging. *Appl Spectrosc*, 58(1):137–40, 2004.

[112] Rogowska J, Bryant CM, and Brezinski ME. Cartilage thickness measurements from optical coherence tomography. *J Opt Soc Am A Opt Image Sci Vis*, 20(2):357–67, 2003.

[113] Sachs JR and Grodzinsky AJ. Electromechanical spectroscopy of cartilage using a surface probe with applied mechanical displacement. *J Biomech*, 28(8):963–76,

1995.

[114] Saïed A, Chérin E, Gaucher H, Laugier P, Gillet P, Floquet J, Netter P, and Berger G. Assessment of articular cartilage and subchondral bone: Subtle and progressive changes in experimental osteoarthritis using 50MHz echography *in vitro*. *J Bone Miner Res*, 12(9):1378–86, 1997.

[115] Samosky JT, Burstein D, Eric Grimson W, Howe R, Martin S, and Gray ML. Spatially-localized correlation of dGEMRIC-measured GAG distribution and mechanical stiffness in the human tibial plateau. *J Orthop Res*, 23(1):93–101, 2005.

[116] Senzig DA, Forster FK, and Olerud JE. Ultrasonic attenuation in articular cartilage. *J Acoust Soc Am*, 92(2 Pt 1):676–81, 1992.

[117] Shingleton WD, Hodges DJ, Brick P, and Cawston TE. Collagenase: A key enzyme in collagen turnover. *Biochem Cell Biol*, 74(6):759–75, 1996.

[118] Shull PJ and Tittmann BR. Ultrasound. In Shull PJ, editor, *Nondestructive Evaluation: Theory, Techniques, and Applications*, pages 63–192. Marcel Dekker Inc., New York, USA, 2002.

[119] Spriet MP, Girard CA, Foster SF, Harasiewicz K, Holdsworth DW, and Laverty S. Validation of a 40 MHz B-scan ultrasound biomicroscope for the evaluation of osteoarthritis lesions in an animal model. *Osteoarthritis Cartilage*, 13(2):171–9, 2005.

[120] Stuart MJ and Lubowitz JH. What, if any, are the indications for arthroscopic debridement of the osteoarthritic knee? *Arthroscopy*, 22(3):238–9, 2006.

[121] Suh JK, Youn I, and Fu FH. An *in situ* calibration of an ultrasound transducer: A potential application for an ultrasonic indentation test of articular cartilage. *J Biomech*, 34(10):1347–53, 2001.

[122] Sun DD, Guo XE, Likhitpanichkul M, Lai WM, and Mow VC. The influence of the fixed negative charges on mechanical and electrical behaviors of articular cartilage under unconfined compression. *J Biomech Eng*, 126(1):6–16, 2004.

[123] Töyräs J, Laasanen MS, Saarakkala S, Lammi MJ, Rieppo J, Kurkijärvi J, Lappalainen R, and Jurvelin JS. Speed of sound in normal and degenerated bovine articular cartilage. *Ultrasound Med Biol*, 29(3):447–54, 2003.

[124] Töyräs J, Rieppo J, Nieminen MT, Helminen HJ, and Jurvelin JS. Characterization of enzymatically induced degradation of articular cartilage using high frequency ultrasound. *Phys Med Biol*, 44(11):2723–33, 1999.

[125] Verzijl N, DeGroot J, Bank RA, Bayliss MT, Bijlsma JW, Lafeber FP, Maroudas A, and TeKoppele JM. Age-related accumulation of the advanced glycation endproduct pentosidine in human articular cartilage aggrecan: the use of pentosidine levels as a quantitative measure of protein turnover. *Matrix Biol*, 20(7):409–17, 2001.

[126] Wang CC, Chahine NO, Hung CT, and Ateshian GA. Optical determination of anisotropic material properties of bovine articular cartilage in compression. *J Biomech*, 36(3):339–53, 2003.

[127] Wells PNT. *Physical Principles of Ultrasonic Diagnosis.* Academic Press, London, 1969.

[128] Wilson W, van Donkelaar CC, van Rietbergen R, and Huiskes R. The role of computational models in the search for the mechanical behavior and damage mechanisms

of articular cartilage. *Med Eng Phys*, 27(10):810–26, 2005.

[129] Wong M, Ponticiello M, Kovanen V, and Jurvelin JS. Volumetric changes of articular cartilage during stress relaxation in unconfined compression. *J Biomech*, 33(9):1049–54, 2000.

[130] Xia Y, Moody JB, Burton-Wurster N, and Lust G. Quantitative *in situ* correlation between microscopic MRI and polarized light microscopy studies of articular cartilage. *Osteoarthritis Cartilage*, 9(5):393–406, 2001.

[131] Yamagata T, Saito H, Habuchi O, and Suzuki S. Purification and properties of bacterial chondroitinases and chondrosulfatases. *J Biol Chem*, 243(7):1523–1535, 1968.

[132] Yelin E and Callahan LF. The economic cost and social and psychological impact of musculoskeletal conditions. National Arthritis Data Work Groups. *Arthritis Rheum*, 38(10):1351–62., 1995.

[133] Zhang M, Zheng YP, and Mak AFT. Estimating the effective Young's modulus of soft tissues from indentation tests - Nonlinear finite element analysis of effects of friction and large deformation. *Med Eng Phys*, 19(6):512–7, 1997.

[134] Zheng YP and Mak AF. An ultrasound indentation system for biomechanical properties assessment of soft tissues *in-vivo*. *IEEE Trans Biomed Eng*, 43(9):912–8, 1996.

[135] Zheng YP, Mak AF, Lau KP, and Qin L. An ultrasonic measurement for *in vitro* depth-dependent equilibrium strains of articular cartilage in compression. *Phys Med Biol*, 47(17):3165–80, 2002.

[136] Zheng YP, Niu HJ, Arthur Mak FT, and Huang YP. Ultrasonic measurement of depth-dependent transient behaviors of articular cartilage under compression. *J Biomech*, 38(9):1830–7, 2005.

[137] Zheng YP, Shi J, Qin L, Patil SG, Mow VC, and Zhou KY. Dynamic depth-dependent osmotic swelling and solute diffusion in articular cartilage monitored using real-time ultrasound. *Ultrasound Med Biol*, 30(6):841–9, 2004.

Kuopio University Publications C. Natural and Environmental Sciences

C 185. Luomala, Eeva-Maria. Photosynthesis, chemical composition and anatomy of Scots pine and Norway spruce needles under elevated atmospheric CO2 concentration and temperature.
2005. 137 p. Acad. Diss.

C 186. Heikkinen, Lasse M. Statistical estimation methods for electrical process tomography.
2005. 147 p. Acad. Diss.

C 187. Riihinen, Kaisu. Phenolic compounds in berries.
2005. 97 p. Acad. Diss.

C 188. Virkutyte, Jurate. Heavy metal bonding and remediation conditions in electrokinetically treated waste medias.
2005. 133 p. Acad. Diss.

C 189. Koistinen, Kaisa. Birch PR-10c: multifunctional binding protein.
2006. 79 p. Acad. Diss.

C 190. Airaksinen, Sanna. Bedding and manure management in horse stables: its effect on stable air quality, paddock hygiene and the compostability and utilization of manure.
2006. 91 p. Acad. Diss.

C 191. Asikainen, Arja. Use of computational tools for rapid sorting and prioritising of organic compounds causing environmental risk with estrogenic and cytochrome P450 activity.
2006. 51 p. Acad. Diss.

C 192. Ålander, Timo. Carbon composition and volatility characteristics of the aerosol particles formed in internal combustion engines.
2006. 54 p. Acad. Diss.

C 193. Molnaŕ, Ferdinand. Structural analysis of the ligand-binding domains of human and mouse CAR, human VDR and human PPARs.
2006. 115 p. Acad. Diss.

C 194. Kasurinen, Anne. Soil-related processes of young silver birch trees grown under elevated CO_2 and O_3.
2006. 64 p. Acad. Diss.

C 195. Metsärinne, Sirpa. Degradation of Novel and Conventional Complexing Agents.
2006. 138 p. Acad. Diss.

C 196. Heijari, Juha. Seed origin, forest fertilization and chemical elicitor influencing wood characteristics and biotic resistance of Scots pine.
2006. 39 p. Acad. Diss.

C 197. Hakulinen, Mikko. Prediction of density, structure and mechanical properties of trabecular bone using ultrasound and X-ray techniques.
2006. 84 p. Acad. Diss.

C 198. Al Natsheh, Anas. Quantum Mechanics Study of Molecular Clusters Composed of Atmospheric Nucleation Precursors.
2006. 55 p. Acad. Diss.